



# Complex precursory activity prior to the c.7600 yr BP Mazama (Crater Lake, USA) eruption

 Hannah M. Buckland<sup>\*α,β</sup>,  Katharine V. Cashman<sup>α,γ</sup>, Jessica J. Rawlings<sup>α,δ</sup>, Lilli Day<sup>α,ε</sup>, and Simon Young<sup>ζ</sup>

<sup>α</sup> School of Earth Sciences, University of Bristol, Wills Memorial Building, Bristol, UK.

<sup>β</sup> Department of Geography, Swansea University, Singleton Campus, Swansea, UK.

<sup>γ</sup> Department of Earth Sciences, University of Oregon, Eugene, OR, USA.

<sup>δ</sup> National Oceanography Centre, University of Southampton, Southampton, UK.

<sup>ε</sup> Scottish Universities Environmental Research Centre, University of Glasgow, Glasgow, UK.

<sup>ζ</sup> Lancaster Environment Centre, University of Lancaster, Lancaster, UK.

## ABSTRACT

Large magnitude explosive volcanic eruptions occur globally at a rate of 1–2 per 1000 years and can cause devastating global impacts. Despite the risk these eruptions pose, we have no reliable method to forecast whether lower magnitude eruptions are precursory to a larger event. Here we use deposits from the ~7.6 ka eruption of Mount Mazama (Crater Lake, Oregon) to analyze precursors to a large eruption. New compositional and textural data suggest that deposits formerly attributed to the climactic eruption include at least three precursor eruptions. In this way, the climactic Mazama eruptive sequence resembles the four-month build-up to the 1883 Krakatau eruption. Distinctive textural and compositional properties of precursor units further suggest that at least one precursory eruption tapped a separate magma lens. Together our data support the growing evidence that eruption of large magma volumes requires the pre- or syn-eruptive amalgamation of multiple melt lenses.

**KEYWORDS:** Precursory eruption; Textural analysis; EPMA; SEM; Crater Lake; Large magnitude eruption.

## 1 INTRODUCTION

A major challenge in volcanology is translating precursory activity into accurate eruption forecasts [Decker 1986; Sparks 2003; Wright et al. 2019]. Correct interpretation of precursory signals is particularly critical for very large (magnitude >M7) caldera-forming eruptions that cause devastating global impacts [Newhall et al. 2018; Cassidy and Mani 2022]. The most recent such eruption—Tambora, Indonesia, 1815—was responsible for at least 60,000 fatalities [Auker et al. 2013], famously caused a ‘year without a summer’ in the northern hemisphere, may have initiated the first worldwide cholera pandemic and, over the longer term, may have laid the foundation for Ireland’s great famine and the first economic depression in the US [D’Arcy Wood 2015]. The consequences of the next M7 eruption will certainly be even more wide-ranging, as illustrated by the supply chain disruption created by the much smaller (M4) 2010 eruption of Eyjafjallajökull, Iceland [Birtchell and Büscher 2010; Harris et al. 2012]. The long repose period between >M7 eruptions [Rougier et al. 2018], however, means that we have limited knowledge about the sequence of events that may presage a caldera-forming event.

Recent work on past eruptions has provided evidence that the build-up to a caldera-forming event may escalate over at least months and involve multiple explosions. For example, the M6.1 eruption of Pinatubo, Philippines, in 1991 was preceded by ~2 months of precursory activity that included earthquakes, phreatic eruptions, dome extrusion and, over the last few days, various forms of explosive activity [Hoblitt 1996]. The onset of activity preceding the M6.7 eruption of Krakatau

volcano, in 1883, was well documented by Dutch and British researchers [Simkin and Fiske 1983]. A poorly known sub-Plinian (?) – to – effusive eruption in 1680–81 may have been an early precursor [Verbeek 1885]; better documented precursory activity included several years of seismicity [Symons 1888] and ~4 months of precursory Vulcanian/sub-Plinian eruptions (probably in part phreatomagmatic). Near-continuous ash emissions then preceded eruptions from multiple vents that intensified during the days leading to the paroxysmal activity producing ash fall over tens of kilometres [Madden-Nadeau et al. 2021]. The build-up to the M7 eruption of Tambora volcano, Indonesia, in 1815 is not as well documented, although hints of precursory activity found in ship logs suggest volcanic unrest as early as 1812, then clear ash-producing eruptions in 1814 [Stothers 1984]. An ~M5 eruption on 5 April 1815 lasted for several hours before the main phase of the eruption began at 7 pm on 10 April with three separate eruption columns initially observed near the volcano’s summit [Stothers 1984]. Although there are no eyewitness accounts for the late-seventeenth century BCE eruption of Santorini volcano (the M7.3 Minoan eruption), geologic evidence indicates that there were early alternating magmatic and phreatomagmatic sub-Plinian eruptions [Cioni et al. 2000] prior to multiple Plinian phases that alternated in eruptive style as the vent migrated into the pre-existing flooded caldera [Druitt 2014]. A recent study of the M8.3 Huckleberry Ridge eruption, Yellowstone, provides evidence not only of multiple eruptions in the early Plinian phase of activity but also tapping of multiple melt lenses [Myers et al. 2016]. Finally, the 15 January 2022 M6.2 eruption of Hunga Tonga-Hunga Ha’apai volcano was preceded by eruptions in 2009 and 2014–2015, as well as two

\*✉ h.m.buckland@swansea.ac.uk

sub-Plinian eruptions in the month leading up to the main eruption that sent a spectacular umbrella cloud to ~53 km a.s.l. [Global Volcanism Program 2022; Gupta et al. 2022; Kelly et al. 2024]. Taken together, these examples show that the onset of caldera-forming eruptions can be protracted and complex; these examples also raise important questions about both the evolving geometry of the magma reservoir feeding successive events and the physical processes required to fully destabilize complex magmatic systems.

Here we re-examine deposits from the onset of climactic activity during the ~7600 yr BP [Zdanowicz et al. 1999; Egan et al. 2015] eruption of Mount Mazama that produced Crater Lake, Oregon, with the goal of assessing conditions that triggered the paroxysmal phase. The Mazama eruption had a magnitude  $\geq M7.1$ , deposited ash over >1 million km<sup>2</sup> of north-western North America [Buckland et al. 2020] and caused extensive and long-lasting impacts on the surrounding landscape and vegetation [e.g. Long et al. 2014; O'Connor et al. 2015; Baig and Gavin 2023] and, in some locations, the Indigenous communities [Oetelaar and Beaudoin 2005; 2016]. The Mazama tephra deposit offers a unique opportunity to study the run-up to an >M7 eruption because of the predominantly terrestrial deposition and the exceptional preservation of the Plinian fall sequence. The caldera-forming eruption had multiple precursor eruptions during the c.200 years leading to the climactic event, two of which produced Llao Rock and Cleetwood fall deposits [Bacon 1983; Young 1990; Wiejaczka and Giachetti 2022]. Both initiated with strong explosive activity and ended with effusion of substantial rhyodacite lava flows. More surprisingly, the rhyodacite flow that followed the Cleetwood explosive activity was still hot when the Crater Lake caldera formed [Bacon 1983], suggesting a repose interval of only weeks to months. What then triggered the main phase of the eruption? We address this question by examining, in detail, the early climactic activity, which has been separated into two main phases—the lower pumice and upper pumice units—discriminated by their different dispersal directions and separated by a prominent ash bed [Young 1990]. We focus particularly on the ash fraction of medial deposits, building on studies of recent, smaller eruptions that have demonstrated how ash textures can provide information about subsequent eruption magnitude [Hammer et al. 1999; Taddeucci et al. 2004; Suzuki et al. 2013; Gaunt et al. 2016; Matsumoto and Geshi 2021; Wright et al. 2023]. Importantly, such analysis has not yet been used to interpret the build-up to large prehistoric eruptions.

## 2 BACKGROUND

### 2.1 The ash component of tephra deposits

Typically, petrologists analyse the larger (lapilli-size) components of tephra deposits while physical volcanologists pay more attention to the ash-sized components. This division derives, on the one hand, from the petrologic opportunity provided by large pumice clasts to constrain conditions of pre-eruptive magma storage and ascent [e.g. Blundy and Cashman 2008; Saunders et al. 2012; Cooper and Kent 2014; Shamloo and Till 2019] and, on the other, the volumetric dominance of ash and its importance for understanding conditions of magma

fragmentation, ash transport and deposition [e.g. Rosi et al. 1999; Pistolesi et al. 2011; Cioni et al. 2014; Eychenne et al. 2015; Pistolesi et al. 2015; Buckland et al. 2021; 2022]. Importantly, however, textural analysis of the ash component can also provide insight into conduit processes related to decompression and temporary arrest, particularly when constrained by experiments [e.g. Hammer et al. 1999; Cashman and McConnell 2005; Miwa et al. 2013; Cioni et al. 2014; Cassidy et al. 2015; Gaunt et al. 2016; Liu et al. 2020; Váscónez Müller et al. 2022]. Data compilation of samples from sequential eruptions with known preceding repose times shows that, in general, plagioclase microlite crystallinity increases with increasing pre-eruptive repose duration and that the maximum crystal number per area ( $N_A$ ) correlates crudely with explosivity (as measured by VEI or column height; [Clarke et al. 2007; Bain et al. 2019; Wright et al. 2023]), although melt composition (viscosity) also plays a role. Additional measurements of volatile contents in either melt inclusions [e.g. Bouvet de Maisonneuve et al. 2012; Cassidy et al. 2016; Stock et al. 2016; Ruth et al. 2018; Wright et al. 2023] or matrix glass [e.g. Edmonds 2001; Cashman and McConnell 2005; Wright et al. 2007; Myers et al. 2014] can help to assess pre-eruptive storage pressures within a conduit; zoning patterns of crystal rims can further refine magma storage and ascent history [e.g. Allan et al. 2013; Coote and Shane 2016; Váscónez Müller et al. 2022; Wright et al. 2023].

### 2.2 Mazama eruption

#### 2.2.1 Constructing a magma reservoir

The magma reservoir that ultimately produced the climactic eruption was constructed over 40–50 ka [Bacon and Druitt 1988; Karlstrom et al. 2015]. The evolution of the growing magma reservoir is evidenced by at least three small rhyodacite eruptions between ~27 and 18 ka that represents leaks from the system. Andesitic enclaves preserved information on the mafic inputs to the system and are classified chemically as low-Sr (LSr), in comparison to later high-Sr (HSr) andesitic inputs. LSr enclaves are notable in having <sup>238</sup>U-excess, which is rare in Cascade lava and suggests melting and assimilation of hydrothermally altered upper crust [Ankney et al. 2013]. Additional support of the importance of hydrothermal alteration in developing the climactic magmatic system comes from O isotope data [Bacon et al. 1994]. Spatial patterns of eruptive activity further suggest that during this time period the bulk magma input into the system increased because of both an increase in deep magma flux and an expanding zone of dike capture created by the growing magmatic system [Karlstrom et al. 2015].

#### 2.2.2 Eruption precursors

Knowledge of the 7627 ± 150 yr BP [Zdanowicz et al. 1999] Mazama eruption and its precursors rests primarily on foundational work by Bacon and co-workers [e.g. Bacon 1983; Bacon and Druitt 1988; Druitt and Bacon 1989; Bacon et al. 1992; Mandeville et al. 2009]. This work demonstrated that the largest and most explosive precursory eruptions were those of Llao Rock and Cleetwood.

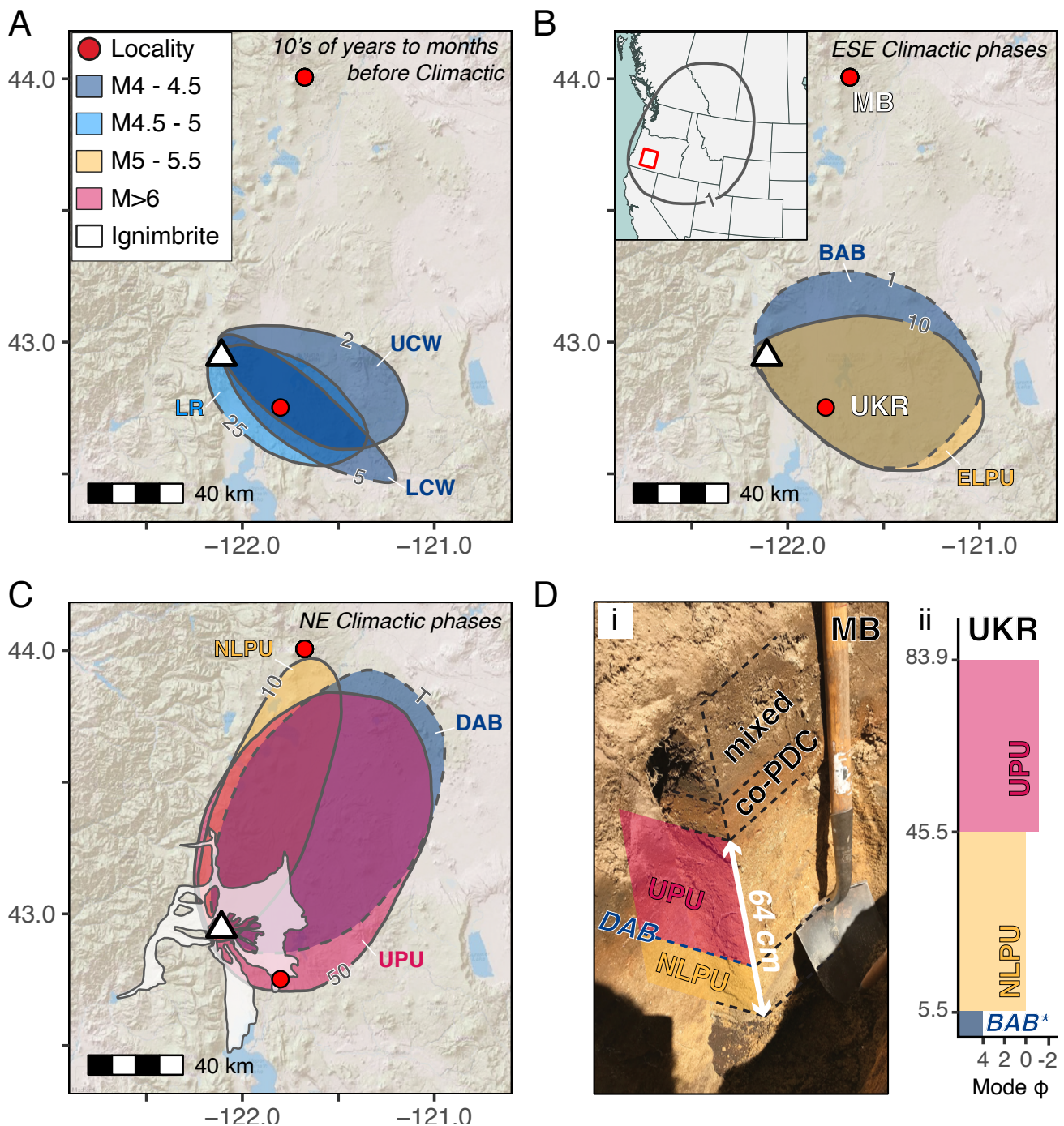


Figure 1: Main tephra fall units from precursory and the climactic Mazama eruptions. The thinnest mapped isopach of each eruptive phase is shown in panels [A]–[C], each isopach is labelled with the thickness reported in cm or T representing trace amount. The fill colour of each isopach corresponds to the eruption magnitude [ $M = \log_{10}(\text{erupted mass}) - 7$  Pyle 2000], as shown in the legend in panel [A] and inferred from Young [1990]. Two key localities referred to in this study are shown as red circles in panel [B], Mount Bachelor (MB) and Upper Kirk Road (UKR). Panel [B] also contains an inset map showing the position of panels [A]–[C] (red square) in relation to the distal Mazama deposit [Buckland et al. 2020]. [A] Isopachs for the Llaor Rock [Young 1990], Lower Cleetwood (LCW) and Upper Cleetwood (UCW [Wiejaczka and Giachetti 2022]). [B] Isopachs for the climactic units dispersed ESE from the vent; the basal ash bed (BAB) and eastern lower pumice unit (ELPU [Young 1990]). [C] Isopachs of the northern lower pumice unit (NLPU), divider ash bed (DAB) and upper pumice unit (UPU [Young 1990]). Also shown is the outline of the ignimbrite deposit that was deposited in the final phase of the climactic eruption [Williams 1942]. [D] i) Annotated photograph of the tephra section at Mount Bachelor showing the NE dispersed units (NLPU, UPU, and trace DAB); ii) Sketch stratigraphic log of auger recovered samples from Upper Kirk Road with absolute thicknesses used from equivalent site 47 in Young [1990]. \*BAB was not recovered in this study as our sampling method was not sufficiently precise to sample the 5.5 cm thick deposit.

Llao Rock issued from a vent on the NW rim of the current caldera (Figure 1A). Carbon dates suggest that the eruption preceded the climactic event by up to 200 years, but recent analysis of a high-resolution lake core refines this estimate to ~75 years [Baig and Gavin 2023]. The eruptive deposits, which are relatively fine-grained [Young 1990], include a pumice fall deposit to the SE (>2 km<sup>3</sup> bulk volume; Young [1990]; Figure 1A) followed by a large (0.5 km<sup>3</sup> DRE [dense rock equivalent]) rhyodacite flow. Proximal deposits are zoned in composition, with early-erupted magma significantly more evolved, hornblende-rich and more depleted in volatiles (S and Cl) than the later Cleetwood and climactic eruptions [Bacon and Druitt 1988; Mandeville et al. 2009]. This LSr magma body that fed this eruption is assumed to have resided at a relatively shallow level NW of the main magma body. The associated lava flow is unusually enriched in vesicular HSr andesite inclusions, which represent a new and distinct mafic input into a shallow (and partially degassed) reservoir [Bacon and Druitt 1988].

The Cleetwood vent lies on the NE rim of the current caldera [Bacon 1983] and produced two explosive phases documented by a well-defined Plinian fall deposit (~0.7–1 km<sup>3</sup> DRE) ESE of the vent [Young 1990; Wiejaczka and Giachetti 2022, Figure 1A] which was followed by a 0.6 km<sup>3</sup> rhyodacitic lava flow [Bacon 1983]. The Cleetwood rhyodacite also includes HSr andesite enclaves that represent at least two different mafic inputs into the magmatic system [Bacon and Druitt 1988]. A range of Sr isotope compositions confirms the diversity of parent magmas [Bacon et al. 1994]. Examination of the 20 m-thick proximal tephra sequence immediately underlying the lava flow shows variations in tephra components and grain size consistent with an unsteady eruption [Bacon 1983; Young 1990; Bourgeois 1998]. Constituent pumice clasts preserve a wide range of microlite textures (number density, size distribution and overall crystallinity) that testify to decompression paths that varied throughout the eruption sequence [Bourgeois 1998; O'Donnell and Gardner 2022]. The erupted magma is compositionally identical to that erupted from the climactic magma reservoir [Bacon and Druitt 1988]. Welding of climactic pumice on the still-hot Cleetwood rhyodacite flow and slumping of that flow into the newly formed caldera demonstrate that the climactic eruption sequence initiated shortly after the Cleetwood activity [Bacon 1983; Kamata et al. 1993]. A puzzling question, then, is why the Cleetwood eruption ended with lava effusion, and why the climactic eruption initiated within weeks to months from a nearby vent.

### 2.2.3 The climactic eruption sequence

The climactic eruptive sequence has been divided into single vent and ring vent phases [Bacon 1983]. The single vent phase started with deposition of a phreatomagmatic basal ash bed (BAB; Figure 1B); this was followed by two separate Plinian phases that generated the lower (LPU) and upper (UPU) pumice fall units, which are distinguished not only by their different aerial distributions (Figure 1), but also by the distinctive 'salt-and-pepper' texture of the LPU [Young 1990]. The LPU was mapped as bilobate by Young [1990] as no stratigraphic section preserved the LPU as two distinct units sepa-

rated by either a change in texture or grain size. By this assessment, the LPU lies well within the Plinian field of Pyle [1989]. Overlying the northern lobe of the lower pumice (NLPU) is an intervening divider ash bed (DAB) (Figure 1C; Young [1990]). The DAB is inferred to represent a temporary eruptive pause; however, the origin of pause is unknown. Magma erupted during the single vent phase is compositionally uniform rhyodacite, with only minor inclusions of HSr andesitic scoria.

Taken together, the petrology and field data suggest that the evolution of the climactic magma reservoir included periodic recharge by, and subsequent fractionation of, at least two distinct andesitic magmas, one HSr and one LSr. Contributions of these two recharge magmas to the evolved rhyodacite are evident in both bulk magma compositions and the variable Sr content of plagioclase at constant anorthite content. LSr recharge magma supplied the earliest precursory eruptions (including the explosive component of the Llao Rock eruption); HSr recharge magma is present as enclaves in the Llao Rock magma and dominates the late precursory and climactic eruptive sequence. These data have been incorporated into a conceptual model of the magma reservoir as a sill-like melt lens overlying a crystal mush, which is periodically recharged at the mush-melt interface by either HSr or LSr andesite [Wright et al. 2012]. Studies of phenocryst-hosted melt inclusions provide further evidence of late-stage recharge of HSr andesitic melt (with associated high H<sub>2</sub>O and S [Bacon et al. 1992; Mandeville et al. 2009]). Perhaps more surprising is evidence for substantial open system degassing prior to the climactic eruption, evidence that includes (1) an apparent absence of trapped CO<sub>2</sub> in melt inclusions from Cleetwood and climactic pumice, and (2) isotopic evidence that as much as 50 % of the S component could have been lost by pre-eruptive open-system degassing. Also interesting is the wide range in melt inclusion dissolved water contents (3–7 wt.%), which yield saturation pressures equivalent to a depth range of 4–12 km for pyroclasts from precursory, as well as climactic, activity. A fundamental question is whether these data record eruption storage depths immediately prior to eruption or whether the melt inclusions were trapped early, and the host crystals later transported to shallow levels.

## 3 METHODS

To improve our understanding of the onset of the climactic eruption, we analysed ash samples from both the eastern (ELPU) and northern (NLPU) lobes of the LPU, the DAB, and the UPU.

### 3.1 Field sampling and laboratory preparation

We investigated the Mazama fall deposits at two key sites (Figure 1). At the Mount Bachelor site, we dug a 1.5 m-deep tephra pit where we observed two well-sorted fall deposit units, the NLPU and the UPU (Figure 1D), as well as a thin (<1 cm) ash-rich horizon between the two fall units correlating to the DAB. Here the base of the NLPU is in direct contact with a layer of black scoria and the top of the UPU is overlain by a fine-grained unit (co-ignimbrite ash) that grades into a mixture of tephra and topsoil (Figure 1Di). The Upper Kirk Road site (Figure 1) was included to examine the ELPU. Here we

used an auger to sample the deposit because of the thickness of the overlying ignimbrite. To ensure that we sampled the ELPU, we correlated changes in the componentry and grain size of the material we retrieved in the field to thickness, grain size and componentry data collected by Young [1990] at three locations near the Upper Kirk Road site (sites 46, 47, and 58 in Young [1990]; Figure 1Dii). We were confident that we had reached and sampled the ELPU when we recovered the distinctive salt and pepper fine-grained pumice lapilli. Here the ELPU lies below 38 cm of coarser grained yellow to white pumice-dominated lapilli in the UPU.

All samples were dried in a 60 °C oven overnight and split to obtain an aliquot for analysis. We manually dry-sieved the samples of  $-3$  to  $3\Phi$  (8 mm to 125  $\mu\text{m}$ ) in half- $\Phi$  intervals to quantify the coarse grain size distribution by the percentage of mass in each sieve fraction (mass %; see [Supplementary Material 1](#) for complete grain size data). We mounted the coarsest, modal and  $2\Phi$  sieve fractions from each sample in EpoFix resin by Struers then polished the ring mounts to expose particle interiors using diamond suspensions in 9, 3, and 1  $\mu\text{m}$  increments.

### 3.2 Scanning electron microscope (SEM)

All polished mounts were carbon coated and imaged using either the Hitachi S-3500N Scanning Electron Microscope (SEM) at the University of Bristol or the Apreo 25 SEM at the University of Oregon in backscattered electron (BSE) mode. Grid images of the  $2\Phi$  ash mounts were collected for quantitative componentry assessments using a working distance of 16 mm, an accelerating voltage of 15 or 20 kV and typically 100–250 $\times$  magnification, which gave optimal resolution for component identification. Individual, high-resolution BSE images were also collected for particles of interest in each sample from all mounted sieve fractions, particularly ash particles with high microlite contents or other features atypical of climactic Mazama products. We also imaged non-juvenile (holocrystalline) particles, identified based on the absence of matrix glass and commonly, evidence of alteration, and crystals that record complex zoning and or rim growth habits.

We quantified the componentry of the  $2\Phi$  ash (modal grain size) across the different fall units (NLPU, DAB, and UPU) preserved at the Mount Bachelor site from the gridded BSE images. The particles in each sample were assigned one of five categories: phenocrysts, microlite-bearing glass, microlite-free glass, vesicular glass or non-juvenile. Point counting of each particle type was used to calculate the relative proportion of each component in every sample (see [Supplementary Material 1](#) and [Supplementary Material 2](#)). Because of the coarser grain size of the Upper Kirk Road site, the  $2\Phi$  grain size did not represent the mode and therefore a direct comparison with the Mount Bachelor units was not possible. We did, however, examine components in the  $2\Phi$ ,  $1.5\Phi$ , and  $1\Phi$  size classes for comparison (see [Supplementary Material 2](#) for the gridded BSE-SEM images).

Selected BSE images were analysed for matrix plagioclase crystallinity and crystal number density (number per  $\text{mm}^2$ ,  $N_A$ ). The limited grey scale contrast between the crystals and groundmass required outlining the crystals by hand; for this

reason, we limited analysis to characterising the range of textural characteristics. Crystal characteristics were measured using the freeware program Fiji (ImageJ); both plagioclase area fraction (crystallinity) and number density were referenced to the measured groundmass area (excluding vesicles). Crystal shapes were measured by using Fiji to determine the major and minor axes of the best-fit ellipse.

### 3.3 Electron microprobe

Major element glass chemistry was measured by electron probe microanalysis (EPMA) using a JEOL JXA8530F Hyperprobe at the University of Bristol. We analysed a range of groundmass, melt inclusion and embayment glasses. The conditions for analysis were a 5 nA beam current, a 10  $\mu\text{m}$  spot size and an accelerating voltage of 15 kV. All elements were counted on-peak, and the count times were adjusted for each element to minimise beam damage. K, Ca, Si, Na, and Al were analysed first for 10s, Ti and Mg (60 s), and Fe, Mn, Cl (50 s). Secondary standards were analysed at the start and end of each analytical session to ensure that no drift had occurred. Only analyses with totals >97 wt.% were retained and 20–30 individual analyses were collected per sample. All data were normalised to 100 wt.%; totals below 100 wt.% are attributed to secondary hydration, which is common in older tephra deposits [Fontijn et al. 2016; McNamara et al. 2018].

Plagioclase crystals from each unit were analysed using the JEOL Hyperprobe at the University of Bristol. We used two beam currents for analysis. The elements K, Ca, Si, Al, and Na (40 s) were analysed using a 10 nA beam current which was increased to 100 nA for analysing Ti, Mg, Sr and Fe (40 s). All analyses used a 1  $\mu\text{m}$  spot size and an accelerating voltage of 20 kV and all elements were counted on-peak. The SPH Labradorite secondary standard was analysed throughout the duration of data acquisition with no variability or drift observed. At least 12 plagioclase crystal rims were analysed per sample. All major element and crystal composition data are available in [Supplementary Material 1](#), including the secondary standard analyses.

## 4 RESULTS

### 4.1 SEM particle characterisation and image analysis

Ash from the Mount Bachelor site (Figure 1) includes the NLPU, DAB, and UPU (Figure 1). Quantitative componentry classification ([Supplementary Material 1](#)) shows that the NLPU and DAB units contain a significant proportion of microlite-bearing glass (13–25 %) and non-juvenile (12–30 %) components that are not expected in deposits from a large Plinian eruption (Figure 2A–2I). Instead, they are more similar to components of the precursory Llaó Rock and Cleetwood eruptions [Bourgeois 1998; O'Donnell and Gardner 2022]. Additional components include variably vesicular glass, some with highly deformed vesicles, and pronounced narrow rims on plagioclase microlites that indicate rapid late-stage growth. Phenocrysts account for ~30 % of  $2\Phi$  ash in the NLPU and DAB; plagioclase phenocrysts are dominant and typically have rapid growth textures preserved at the outermost rim (Figure 2C, 2I). At this site (~100 km from the eruptive vent), UPU

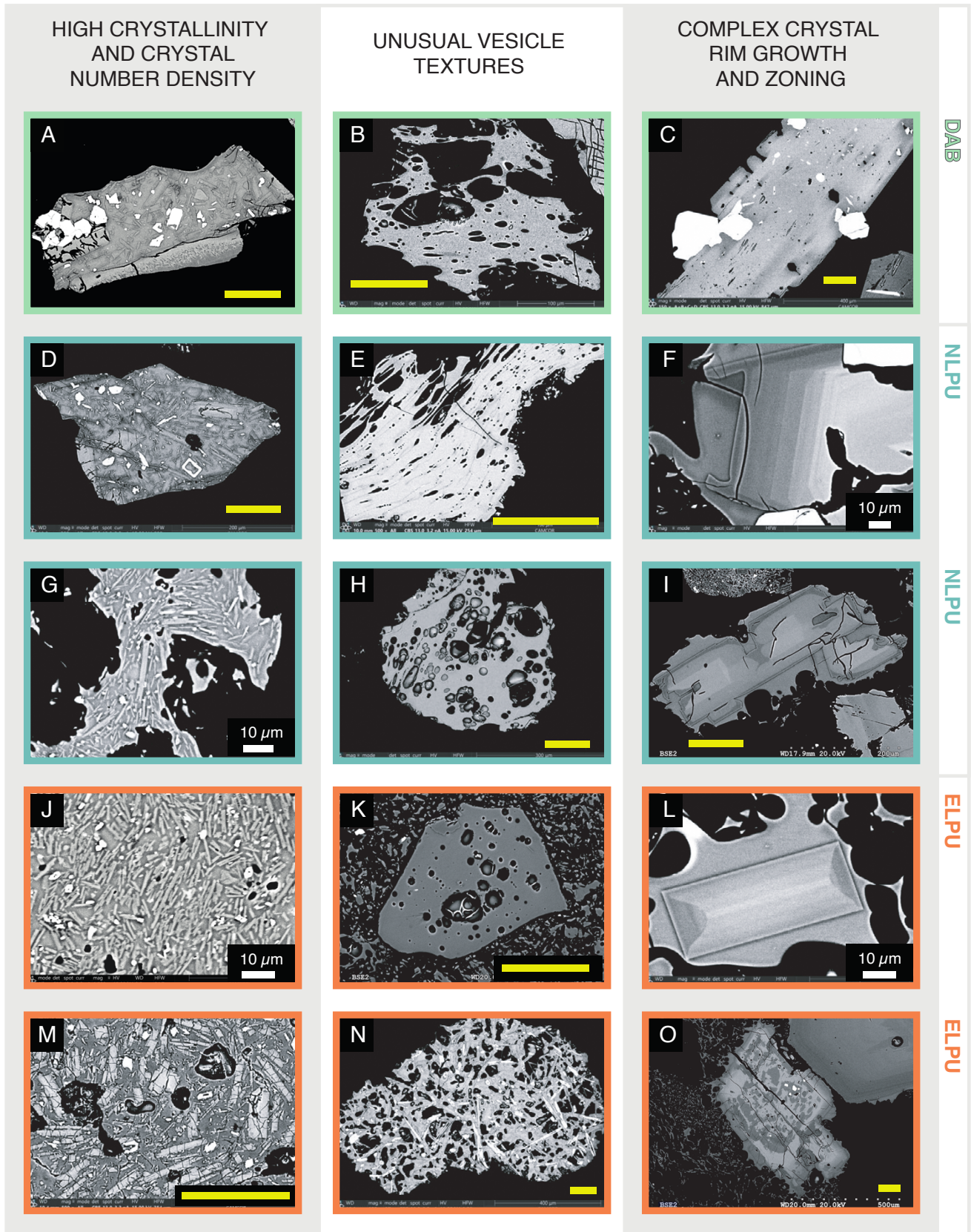


Figure 2: Compilation of BSE images of particles from the lower units (LPU and DAB) of the climactic Mazama eruption. Each column of images relates to the column header; “high crystallinity and crystal number density”, “unusual vesicle textures”, and “complex crystal growth and zoning”. Each row relates to the sub-unit of the climactic tephra which is also shown by the border colour of the image. Yellow scale bars are 100 μm; 10 μm scale bars are in white and are labelled for clarity.

ash has up to 88 % phenocrysts; most are plagioclase and may be either complete or broken and preserve a range of normal and reverse zoning (Supplementary Material 1 and Supplementary Material 2).

Ash from the Upper Kirk Road site was analyzed to characterize emissions from the eastern lower pumice lobe (ELPU; Figure 1). This deposit also includes a range of glassy, microlite-rich and non-juvenile particles (Figure 2). This deposit also includes an ash component that is distinct from those of the NLPU and DAB (Figure 2N). It is characterized by extremely anisotropic crystals of both plagioclase and pyroxene and vesicles that form incipient diktytaxitic textures (see Supplementary Material 2 for additional images). Also unusual are sector-zoned plagioclase, which occur as isolated microphenocrysts (Figure 2L) as well as microlites in the diktytaxitic clasts (Supplementary Material 2).

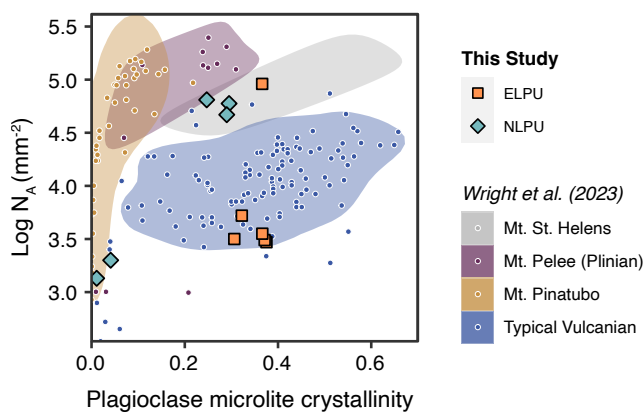


Figure 3: Plagioclase microlite crystallinity versus areal number density of lower pumice unit samples. Large square and diamond symbols are newly collected for this study. Data plotted as small circles are from Wright et al. [2023] and have been grouped according to eruption style and/or the source eruption (please see Wright et al. [2023] for the appropriate references for the crystallinity data).

The plagioclase microlite crystallinity measured from 11 LPU BSE-SEM images ranges from 1 to 41 %, and the areal number density spans one order of magnitude from 1365 to 90,507  $\text{mm}^{-2}$  (see Supplementary Material 1). Interestingly when compared to published ash crystallinity data (Figure 3), we see that all but one of the ash particles analysed from the ELPU overlap with values measured from Vulcanian style eruptions (e.g. eruptions from Galeras, Shinmoedake and Augustine [Wright et al. 2023]). On the other hand, the high NLPU crystallinity and  $N_A$  values are more like those measured from the precursory ash from Mount St. Helens 1980 eruption by Cashman and Hoblitt [2004], Figure 3).

#### 4.2 Glass and plagioclase compositional data

Glass data for the Cleetwood, ELPU, NLPU, and UPU fall units are shown in Figure 4. Data for individual units span different ranges on bivalent element plots. Particularly striking are the different trends recorded in the alkali and  $\text{TiO}_2$  data for the ELPU (Figure 4J, 4K). Specifically, the ELPU spans a wider range of groundmass  $\text{SiO}_2$  (70–77 wt.%) and MgO

(0.05–0.73 wt.%) than the other fall deposits. Here the high  $\text{SiO}_2$ /low MgO groundmass analyses correspond to microlite-bearing glass particles with very high crystallinity (Figure 2M) while the high Cl glass is found exclusively as the matrix of diktytaxitic particles (Figure 2K). Some melt inclusions analysed from the NLPU record >74 wt.%  $\text{SiO}_2$ , which exceeds most matrix glass analyses and is equivalent to the upper  $\text{SiO}_2$  range reported for the evolved Liao Rock pyroclasts [Mandeville et al. 2009]. Cleetwood melt inclusions, in particular, are notable for their Cl range (Figure 4O).

Plagioclase rim compositions are reported by unit in Figure 5. Data from NLPU and DAB ash show little variation, with An ~40 and Sr values <2000 ppm, a LSr characteristic. Data from ELPU ash particles, in contrast, show a much wider range in Sr for similar An contents. Plagioclase with HSr (>2000 ppm) compositions requires recharge by HSr andesite [Druitt and Bacon 1989]. Our data are unusual, however, in preserving an HSr signature at low An contents (~An40); Druitt and Bacon [1989] find that high Sr plagioclase is confined to plagioclase contained within late-erupted HSr scoria with An>50 (Figure 5E). We find similar plagioclase rims in the UPU (Figure 5A), which includes HSr scoria during the final stages of the climactic eruption [Druitt and Bacon 1989].

#### 4.3 Rhyolite-MELTS modelling

We used Rhyolite-MELTS to model the melt evolution of the climactic Mazama products [Gualda et al. 2012, Figure 6]. We ran the thermodynamic model with different starting compositions including whole-rock data from Druitt and Bacon [1989] and the composition of the least evolved groundmass from the ELPU (see Supplementary Material 1). Initial  $\text{H}_2\text{O}$  contents ranged from 4–7 wt.% and calculations were performed under both isothermal (decompression) and isobaric (cooling) conditions. Crystallization paths differ most markedly in the behavior of  $\text{TiO}_2$ , which tracks crystallization of ilmenite. Here isobaric cooling produces a trend of decreasing  $\text{TiO}_2$  with increasing  $\text{SiO}_2$ , which indicates ilmenite fractionation. Only some isothermal runs produced ilmenite (Supplementary Material 1). Comparison with measured glass data shows that isothermal decompression appears to best explain NLPU glass compositions and a subset of ELPU compositions. Isobaric cooling, in contrast, best explains the prominent trend of decreasing  $\text{TiO}_2$  with increasing  $\text{SiO}_2$  that characterizes much of the ELPU glass data (Figure 6).

## 5 DISCUSSION

The data presented above provides evidence that the ash component of deposits from the climactic eruption sequence preserves a record of short-term, and often shallow, conduit processes known to modulate patterns of precursory activity. Here we place that evidence in a stratigraphic context and use these data to suggest that the climactic eruption sequence initiated with at least two Plinian (?) eruptions represented by the eastern and northern lower pumice units that were likely closely spaced in time but from separate vents. The overlying DAB appears to record another, smaller, eruption prior to the final climactic eruption, as represented by the UPU. Distinctive ash textures and compositions found within the ELPU

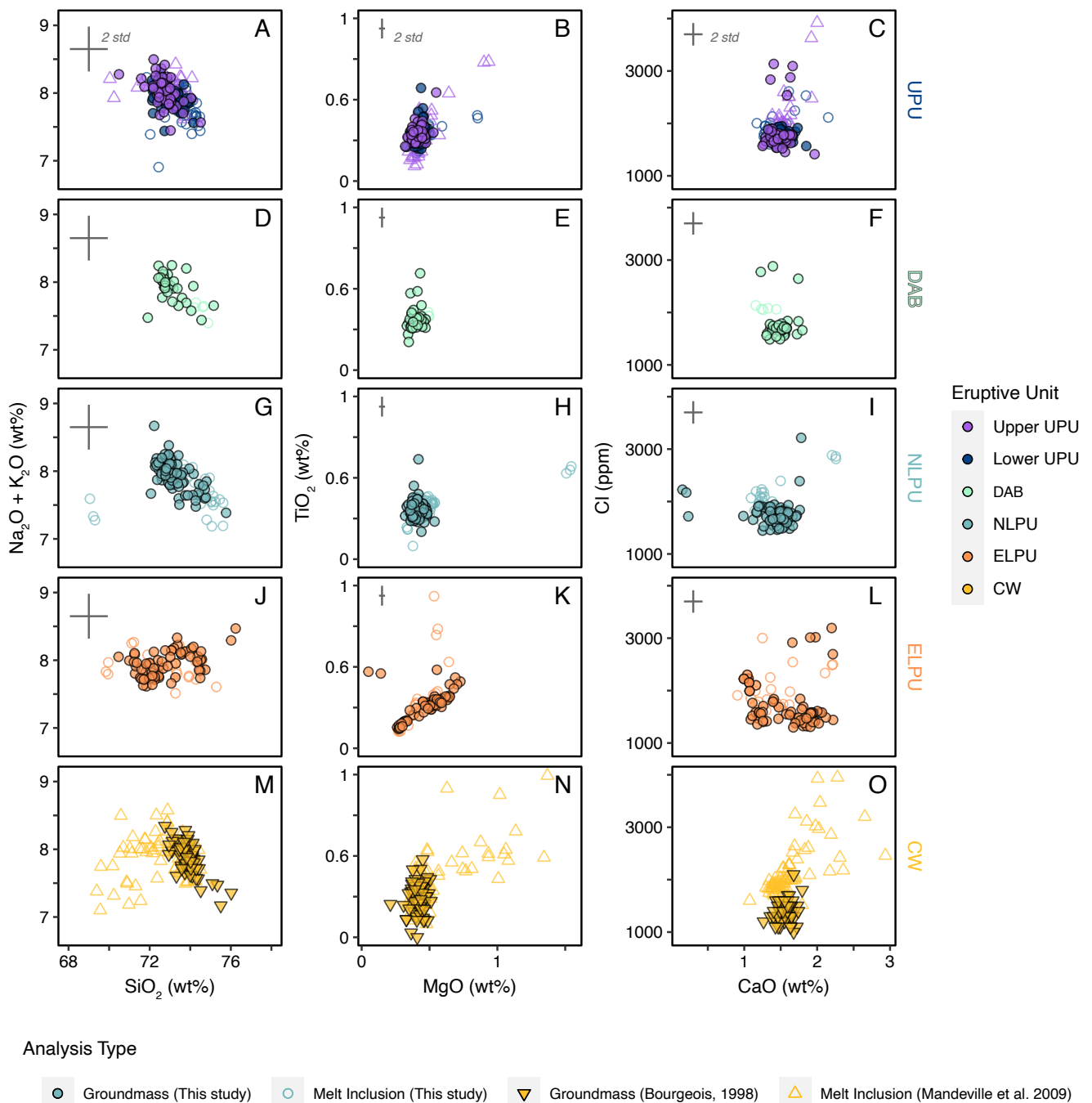


Figure 4: Major and minor element glass geochemistry of subunits within the climactic Mazama eruption. All plots show new data collected for this study as circles and reference data as triangles. Open symbols are melt inclusion analyses whereas filled symbols are groundmass glass analyses. The error bars represent 2 standard deviations of the element as analysed on the Lipari secondary standard. The first column of plots shows  $\text{SiO}_2$  versus  $\text{Na}_2\text{O} + \text{K}_2\text{O}$  (wt.%); the second column shows  $\text{MgO}$  versus  $\text{TiO}_2$  (wt.%); and the third column shows  $\text{CaO}$  (wt.%) against  $\text{Cl}$  (ppm). Each row of plots relates to an eruptive unit which is also distinguished by the symbol colour. The final row of plots (panels [M]–[O]) shows published data for the Cleetwood eruption (CW) from Bourgeois [1998] and Mandeville et al. [2009]. We have assumed that the climactic pumice melt inclusions from Mandeville et al. [2009] are related to the upper UPU and are plotted as open triangles in panels [A]–[C].



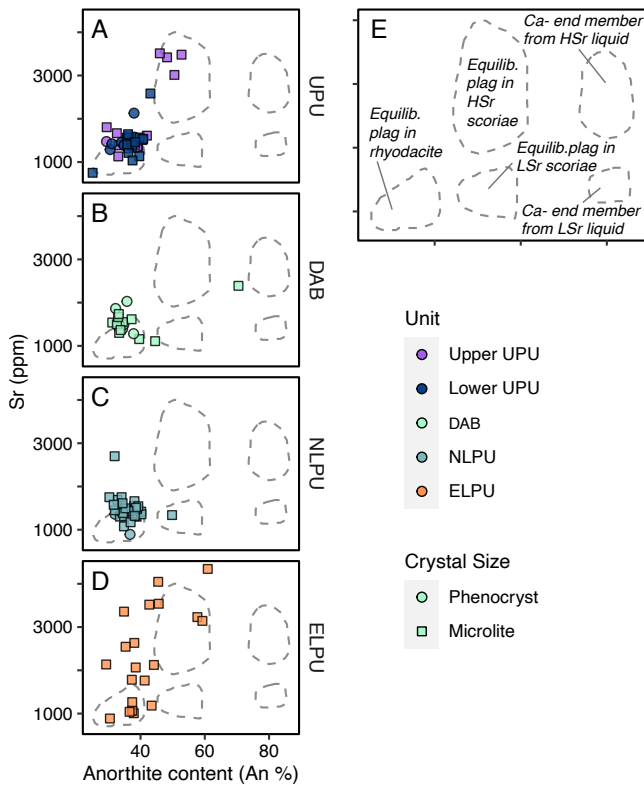


Figure 5: Plagioclase content of climactic sub-units. Each panel shows the Anorthite content (%) and Sr (ppm) data for plagioclase rims from the eruption units [A] UPU; [B] DAB; [C] NLPU and [D] ELPU. Eruptive unit is also shown by the symbol fill colour. The symbol shape indicates the crystal size (phenocryst or microlite). Panel [E] includes labels for the plagioclase compositional zones designated by **Druitt and Bacon [1989]**, see their Figure 6b). The analytical error (2 standard deviations of the element analysed on the SPH Labradorite standard) is within the size of the plotting symbol.

further suggest that this eruption may have tapped a different source than that of the subsequent NLPU and UPU eruptions.

### 5.1 Groundmass textures

Groundmass textures record conditions of magma ascent to the surface [e.g. **Hammer et al. 1999; Cashman and McConnell 2005; Clarke et al. 2007; Martel 2012; Wright et al. 2012; Bain et al. 2019; Preece et al. 2023**]. Plagioclase provides a particularly detailed record of the decompression history of hydrous magma because of its sensitivity to the decreasing water content of the melt with decreasing pressure [**Cashman 1992; Dunbar et al. 1995; Blundy and Cashman 2001; Cashman and Hoblitt 2004; Blundy and Cashman 2005; Cassidy et al. 2015; Waters et al. 2015; Humphreys et al. 2016; Cashman 2020**]. Specifically, the number density of plagioclase crystals (measured as either number per area or number per volume) is a measure of nucleation efficiency, which is a function of both decompression rate and magma composition. The overall abundance of plagioclase (measured as either area or volume fraction) reflects the combined efficiency of crystal nucleation and growth, again a function of decompression rate (time) and

composition (viscosity/element diffusivity). When eruptions are pulsatory, that plagioclase crystallinity corresponds to the duration of the preceding repose interval [**Hammer et al. 1999**]. A recent compilation of plagioclase groundmass textures further suggests that the maximum microlite number density of precursor eruptions increases as the intensity of the climactic eruption increases [**Figure 2 Wright et al. 2023**]. Within this context, the high plagioclase number densities observed in ELPU, NLPU, and DAB ash particles (Figures 2 and 3), as well as in the Cleetwood pumice, indicate a highly pressurized, but discretized, magmatic system. Episodic eruptions from individual vents are inferred from stratigraphic evidence (Cleatwood [**Bourgeois 1998; Wiejaczka and Giachetti 2022**]), mixed microphenocryst and microlite populations in the groundmass (**Figure 2M**; see **Cashman and McConnell [2005]**) and multiple normally zoned growth rims on plagioclase phenocrysts (**Figure 2F**). Observed variations in particle vesicularity provide a record of differential outgassing (**Figure 2B, 2E, 2H, 2K, 2N**) consistent with the evidence of pre-eruptive degassing provided by melt inclusion analyses [**Mandeville et al. 2009**]. Taken together, these data provide a picture of episodic pressure release from different vents, and probably different melt lenses, as the system built toward catastrophic failure (**Figure 7**).

### 5.2 Immediate precursors to the climactic eruption

The sequence of events that immediately preceded the climactic eruption included explosive events that deposited the BAB and ELPU to the SE, overlying deposits of Lla'o Rock and Cleatwood eruptions (**Figure 1B**) and following the modern dominant wind direction at Crater Lake (Mount Mazama [**Buckland et al. 2022**]). Deposits from subsequent eruptions (NLPU, DAB, UPU), in contrast, are to the NNE. This unusual wind direction is most common in the fall (autumn), consistent with inferences of eruption season from pollen analysis [**Mehring et al. 1977**]. Thus, although bilobate deposits can form because of changing wind direction and or plume height during a single eruptive phase (e.g. Hudson 1991 [**Kratzmann et al. 2010**]), we think it more likely that there was a (probably short) time break between deposition of the SE- and NE-dispersed units.

Textural and compositional data further suggest that the ELPU and NLPU eruptions may have been fed from different melt bodies. We base this interpretation on the distinctive characteristics of the subset of ELPU ash particles with 'diktytaxitic' textures (**Figure 2N**). Diktytaxitic textures are common in mafic enclaves, including those in older rhyodacite lava flows from Mazama, and have been used to illustrate conditions of gas-driven filter pressing [**Druitt and Bacon 1986**]. Here rapid cooling during magma recharge into a cooler host creates a network of anisotropic crystals; subsequent gas exsolution and expansion during magma ascent drives residual melt out of the crystal network. Ash particles preserved in ELPU show many of these characteristics. Moreover, notable features of these clasts include the extreme elongation of plagioclase and pyroxene crystals (**Supplementary Material 1**), unusual sector-zoned plagioclase (**Figure 2L, Supplementary Material 2**) and high Cl in the groundmass glass (>2000

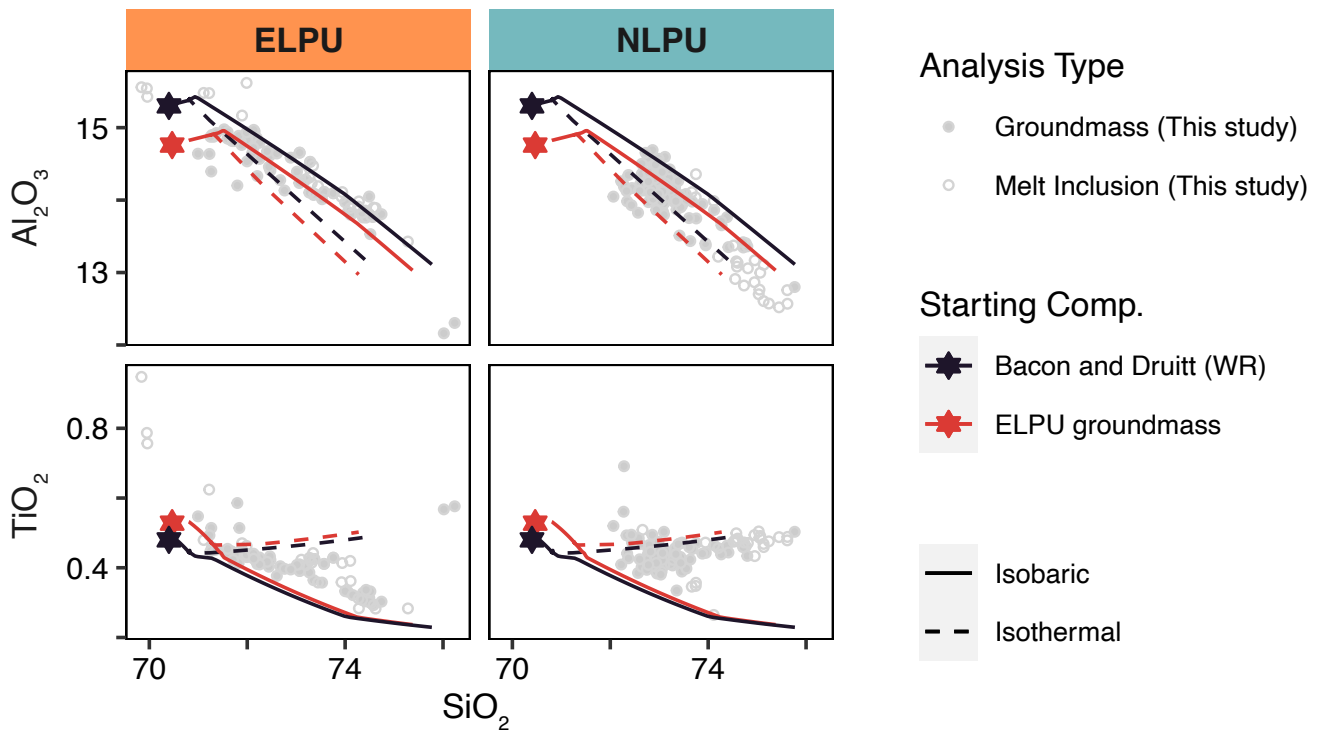


Figure 6: Rhyolite-MELTS liquid lines of descent using different starting compositions and model conditions compared to the glass composition of the LPU. All model runs shown here assumed a starting  $\text{H}_2\text{O}$  content of 5 wt.%. The isobaric runs simulated cooling from 950 to 790 °C at a constant pressure of 200 MPa. The isothermal runs were simulated at a constant temperature of 895 °C and decompressed from 250 to 50 MPa. Details of model runs can be found in [Supplementary Material 1](#). Different starting compositions are shown by different colours and the line type differentiates between isobaric and isothermal runs. The new glass data collected for this study is plotted as grey symbols where the shape represents whether it was a groundmass (filled) or melt inclusion (open) analysis.

ppm; [Figure 4L](#)). These features, together with the incomplete melt expulsion from the crystal network, can be explained by rapid quenching at depth. Quenching at depth is supported by Rhyolite-MELTS modelling ([Figure 6](#)), which indicates that melt in these clasts records isobaric cooling, in contrast to the melt evolution paths subsequent eruptive products, which are better explained by isothermal decompression ([Figure 4](#)).

Another unusual feature of ELPU ash particles is the presence of Hsr plagioclase rims on some of ELPU crystals. Hsr plagioclase rims have been described previously as a feature of in scoria formed from Hsr recharge magma [[Bacon and Druitt 1988](#)]. Unlike these data from scoria phenocrysts, however, Hsr plagioclase rims in ELPU particles have the lower An contents associated with the erupted rhyodacite melt ([Figure 5](#)). Based on this evidence, we suggest that ELPU magma experienced recharge of Hsr magma, most likely in response to withdrawal of magma during the Cleetwood eruption and consequent decompression of the underlying magmatic system ([Figure 7](#)). We further speculate that the ELPU eruption was fed by an isolated or partially isolated melt lens rather than tapping the ‘well-mixed’ homogenous climactic rhyodacitic magma proposed by [Bacon and Druitt \[1988\]](#). This interpretation accords with recent evidence for isolated melt lenses in other magmatic systems that have produced caldera forming eruptions, including Colli Albani [[Vinkler et al. 2012](#)];

Huckleberry Ridge and Lava Creek Tuffs, Yellowstone [[Myers et al. 2016](#); [Shamloo and Till 2019](#)]; Santorini [[Flaherty et al. 2018](#); [2022](#)]; and Krakatau [[Madden-Nadeau et al. 2021](#)].

Overlapping deposits of the NE-dispersed units (NLPU, DAB, UPU) is most easily explained by eruption from the same vent. The NLPU, however, has textural characteristics associated with pulsatory activity, particularly the abundance of microlite-rich ash particles ([Figures 2 and 3](#)). The presence of discrete, thin plagioclase rims further suggests closely spaced explosions (decompression events [[Wright et al. 2023](#)]). Also notable is the incorporation of crystals with evolved melt inclusions ([Figure 4G](#)), which can be explained by disruption of a shallow crystal mush [[Kilgour et al. 2013](#)], perhaps the roof of a larger magma reservoir. The presence of the microlite-rich DAB between the LPU and UPU signals a final eruptive pause ([Figure 7](#)). Repeated closely spaced eruptions are not unusual for the hours to days prior to a caldera-forming eruption; as noted above, similar accelerating activity has been observed prior to climactic eruptions of Krakatau, 1883, Pinatubo, 1991, and Hunga-Tonga, 2022.

A remaining question is why the Cleetwood eruption, and the Llao Rock before it, ended with lava effusion instead of transitioning immediately to the climactic event. Petrologic studies [[Bacon and Druitt 1988](#); [Druitt and Bacon 1989](#)] show that the Llao Rock eruption likely tapped shallow-stored LSr

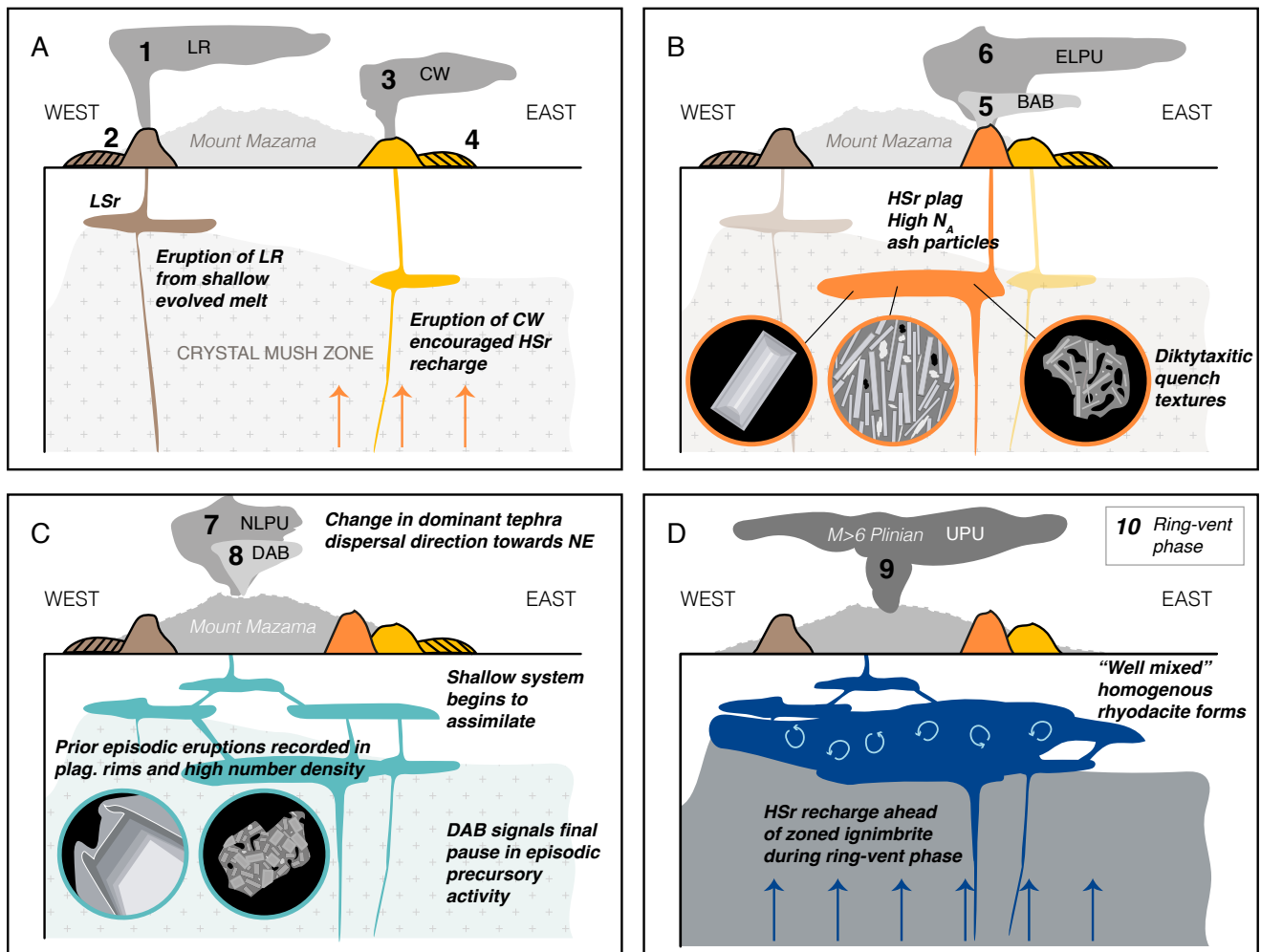


Figure 7: Cartoon diagram of precursory activity at Mount Mazama. The sequence of eruptive activity is numbered 1 to 10. [A] The largest precursory tephra formed eruptions; Llo Rock (LR) and Cleetwood (CW) with associated lava flows (hatched polygons). [B] The eruption of the ELPU from a likely isolated melt lens recording Hsr recharge following the Cleetwood eruption. [C] An abrupt change in dispersal direction and potentially vent location formed the NLPU and DAB likely corresponding to the shallow magmatic storage beginning to assimilate. [D] By the onset of the >M6 Plinian phase (UPU) the 'well-mixed' climactic rhyodacite has amalgamated at depth. Please note this diagram is not to scale and there remains considerable uncertainty in the architecture of the magmatic system that fed the Mazama eruption. Similarly, collapse of the caldera means our understanding of the number and distributions of vents is poor and here we show a simplified, cartoonish reconstruction.

magma (a cupola?) that was compositionally distinct from the Cleetwood and climactic magma. Physical isolation in a shallow melt lens could explain the decrease in overpressure implied by the explosive-to-effusive transition. The appearance of Hsr andesite inclusions within the Llo Rock lava flow provide evidence of new recharge magma, perhaps in response to unloading during the eruption [Karlstrom et al. 2012]. Although it is more difficult to make the same argument for the Cleetwood eruption, given its compositional overlap with the climactic magma and assumed derivation from a large and well-mixed magma reservoir [Bacon and Druiitt 1988; Druiitt and Bacon 1989], the similarities between the two eruptions are striking: both produced substantial tephra deposits ( $>1 \text{ km}^3$ ) and both were followed by effusion of large ( $\geq 0.5 \text{ km}^3$ ) glassy rhyodacite lava flows. It seems reasonable to attribute this behavior to a similar cause (Figure 7). Notably,

in style and erupted volume the Llo Rock and Cleetwood eruptions are similar to recent rhyolite eruptions of Chaiten and Cordon Caulle, Chile. Both produced tephra deposits with volumes  $\sim 1 \text{ km}^3$  and lava flows  $\geq 0.5 \text{ km}^3$ . Both eruptions also lasted approximately one year.

Renewed explosive activity could have been triggered by unloading of the magmatic system because of the Cleetwood eruption. As noted above, it seems plausible that decompression related to unloading promoted recharge of Hsr andesite into the magmatic system the fed ELPU activity. Additional evidence of open-system behaviour prior to the climactic eruption includes reverse zoning of pyroxene crystals [Bacon and Druiitt 1988] and open-system degassing [Mandeville et al. 2009]. Such eruption-induced perturbations to the magmatic system are consistent with accelerated destabilization and amalgamation of melt lenses (Figure 7), as suggested by

detailed studies of other caldera-forming eruptions [e.g. Karlstrom et al. 2012; Vinkler et al. 2012; Cashman and Giordano 2014; Myers et al. 2016; Swallow et al. 2018; Madden-Nadeau et al. 2021].

In summary, whilst our textural and geochemical data provide new insight into the activity that presaged the climactic stage of the Mazama eruption, additional sampling and analysis is required to test our interpretations and better understand the processes that prime a magmatic system that ultimately produces a >M7 eruption. Importantly, our samples were limited to two field sites due to COVID-19 travel restrictions and the termination of funded projects in 2021; testing our hypothesis that the ELPU tapped a distinct melt lens could be achieved by interrogating trace element data from melt inclusions and groundmass glass, diffusion chronometry along crystal zoning patterns and reconstructing the volatile budget of the magmatic system using spectroscopy techniques. Similarly, more comprehensive thermodynamic modelling using rhyolite-MELTS [Gualda et al. 2012] will help reconstruct the pressure, temperature, time ( $P - T - t$ ) histories and phase equilibria for the individual precursory eruptions, again providing an opportunity to test our hypothesis that the ELPU preserves evidence of melt recharge and a different  $P - T - t$  trajectory (Figure 6).

## 6 CONCLUSIONS

Prior studies of the climactic Mazama eruption have focused on the pumice lapilli (>2 mm) for compositional and crystallinity assessments. Here we have shown the value in characterizing the texture and composition of ash particles (<2 mm) in the medial deposits of large magnitude eruptions. For example, in the analyzed samples, high crystal number densities are observed only in the ash fraction of the ELPU and NLP. The same appears to be true for the surge-forming eruptions that preceded the climactic phase of the Pinatubo eruption [Hammer et al. 1999]. Whether this difference is common is difficult to assess, because the internal textures and compositions of ash-sized samples are rarely analyzed. Yet the ash fraction commonly includes contributions from shallow dense plugs, plugs that may be efficiently fragmented at the initiation of each new eruption pulse [Jones et al. 2022]. Deposit characteristics suggest that the immediate run-up to the climactic Mazama eruption included at least two Plinian (~M5) eruptions that form the ELPU and NLP. This adds to the growing body of literature suggesting that large (~M6+) eruptions can generate substantial precursory eruptions before progressing to even larger eruptions. From the geological record it is hard to pinpoint the difference between the Lla Rock eruption, which was followed by a long period of quiescence, and the Cleetwood-ELPU-NLP sequence that was closely followed by the climactic event. The same question arises for Krakatau 1883, which appears to have had a precursory eruption that was similar to Lla Rock in both style and occurrence 1–2 centuries before the caldera-forming event. Both scenarios are concerning for hazard forecasting, as we cannot currently forecast whether a M5 (~1–2 km<sup>3</sup>) eruption is the main event or precursory to a catastrophic eruption. Our research suggests, however, that analysis of precursory

ash deposits may help to track the evolution of subvolcanic systems, including providing evidence of recharge that may precede system destabilization.

## AUTHOR CONTRIBUTIONS

CRedit Author Contributions.

**Conceptualisation:** HMB, KVC; **Methodology:** HMB, KVC, JJR, LD; **Data curation:** HMB, KVC, SY; **Investigation:** all authors; **Formal analysis:** HMB, KVC; **Writing—original draft preparation:** HMB, KVC; **Writing—review and editing:** all authors; **Visualisation:** HMB; **Funding acquisition:** HMB (PhD funding); **Resources:** HMB, KVC (PhD field investigations), SY (PhD field investigations); **Supervision:** HMB & KVC (supervising JJR and LD), KVC (supervising HMB).

## ACKNOWLEDGEMENTS

HMB was supported by a NERC GW4+ Doctoral Training Partnership studentship from the Natural Environment Research Council (NERC; NE/L002434/1) with additional support from the British Geological Survey. KVC acknowledges an AXA Research Fund and a Royal Society Wolfson Merit Award. The manuscript builds on field data collected in the doctoral thesis of SY awarded by the University of Lancaster in 1990. This data was then used and combined with new data in the doctoral thesis of HMB, awarded by the University of Bristol in January 2022. The study was also motivated by new SEM images collected in two MSc theses by JJR and LD awarded by the University of Bristol in January 2022. We would like to thank the early researchers whose extensive work characterising the deposits of the climactic Mazama eruption facilitated this study. We also extend thanks to Dr Ben Buse and Dr Stuart Kearns at the University of Bristol for their assistance with the SEM and EPMA data collection. Finally, we would like to thank three thorough reviewers for helping improve the quality of this manuscript and Dr Nick Varley for his editorial handling.

## DATA AVAILABILITY

The data collected for and used in this study has been shared in the supplementary material.

## COPYRIGHT NOTICE

© The Author(s) 2024. This article is distributed under the terms of the [Creative Commons Attribution 4.0 International License](https://creativecommons.org/licenses/by/4.0/), which permits unrestricted use, distribution, and reproduction in any medium, provided you give appropriate credit to the original author(s) and the source, provide a link to the Creative Commons license, and indicate if changes were made.

## REFERENCES

- Allan, A. S. R., D. J. Morgan, C. J. N. Wilson, and M.-A. Millet (2013). “From mush to eruption in centuries: assembly of the super-sized Oruanui magma body”. *Contributions to Mineralogy and Petrology* 166(1), pages 143–164. DOI: [10.1007/s00410-013-0869-2](https://doi.org/10.1007/s00410-013-0869-2).

- Ankney, M. E., C. M. Johnson, C. R. Bacon, B. L. Beard, and B. R. Jicha (2013). “Distinguishing lower and upper crustal processes in magmas erupted during the buildup to the 7.7 ka climactic eruption of Mount Mazama, Crater Lake, Oregon, using  $^{238}\text{U}$ – $^{230}\text{Th}$  disequilibria”. *Contributions to Mineralogy and Petrology* 166(2), pages 563–585. DOI: [10.1007/s00410-013-0891-4](https://doi.org/10.1007/s00410-013-0891-4).
- Auker, M. R., R. S. J. Sparks, L. Siebert, H. S. Crossweller, and J. Ewert (2013). “A statistical analysis of the global historical volcanic fatalities record”. *Journal of Applied Volcanology* 2(1). DOI: [10.1186/2191-5040-2-2](https://doi.org/10.1186/2191-5040-2-2).
- Bacon, C. R. (1983). “Eruptive history of Mount Mazama and Crater Lake Caldera, Cascade Range, U.S.A.” *Journal of Volcanology and Geothermal Research* 18(1–4), pages 57–115. DOI: [10.1016/0377-0273\(83\)90004-5](https://doi.org/10.1016/0377-0273(83)90004-5).
- Bacon, C. R. and T. H. Druitt (1988). “Compositional evolution of the zoned calcalkaline magma chamber of Mount Mazama, Crater Lake, Oregon”. *Contributions to Mineralogy and Petrology* 98(2), pages 224–256. DOI: [10.1007/bf00402114](https://doi.org/10.1007/bf00402114).
- Bacon, C. R., S. H. Gunn, M. A. Lanphere, and J. L. Wooden (1994). “Multiple Isotopic Components in Quaternary Volcanic Rocks of the Cascade Arc near Crater Lake, Oregon”. *Journal of Petrology* 35(6), pages 1521–1556. DOI: [10.1093/petrology/35.6.1521](https://doi.org/10.1093/petrology/35.6.1521).
- Bacon, C. R., S. Newman, and E. M. Stolper (1992). “Water,  $\text{CO}_2$ , Cl, and F in melt inclusions in phenocrysts from three Holocene explosive eruptions, Crater Lake, Oregon”. *American Mineralogist* 77(9–10), pages 1021–1030.
- Baig, J. and D. G. Gavin (2023). “Postglacial vegetation and fire history with a high-resolution analysis of tephra impacts, High Cascade Range, Oregon, USA”. *Quaternary Science Reviews* 303, page 107970. DOI: [10.1016/j.quascirev.2023.107970](https://doi.org/10.1016/j.quascirev.2023.107970).
- Bain, A. A., E. S. Calder, J. A. Cortés, G. P. Cortés, and S. C. Loughlin (2019). “Textural and geochemical constraints on andesitic plug emplacement prior to the 2004–2010 vulcanian explosions at Galeras volcano, Colombia”. *Bulletin of Volcanology* 81(1). DOI: [10.1007/s00445-018-1260-y](https://doi.org/10.1007/s00445-018-1260-y).
- Birtchnell, T. and M. Büscher (2010). “Stranded: An Eruption of Disruption”. *Mobilities* 6(1), pages 1–9. DOI: [10.1080/17450101.2011.532648](https://doi.org/10.1080/17450101.2011.532648).
- Blundy, J. and K. V. Cashman (2001). “Ascent-driven crystallisation of dacite magmas at Mount St Helens, 1980–1986”. *Contributions to Mineralogy and Petrology* 140(6), pages 631–650. DOI: [10.1007/s004100000219](https://doi.org/10.1007/s004100000219).
- (2005). “Rapid decompression-driven crystallization recorded by melt inclusions from Mount St. Helens volcano”. *Geology* 33(10), page 793. DOI: [10.1130/g21668.1](https://doi.org/10.1130/g21668.1).
- (2008). “Petrologic Reconstruction of Magmatic System Variables and Processes”. *Reviews in Mineralogy and Geochemistry* 69(1), pages 179–239. DOI: [10.2138/rmg.2008.69.6](https://doi.org/10.2138/rmg.2008.69.6).
- Bourgeois, R. L. (1998). “Physical characteristics of proximal Cleetwood airfall Deposits, Crater Lake, OR: The transition from explosive to effusive eruption”. PhD thesis. University of Oregon.
- Bouvet de Maisonneuve, C., M. Dungan, O. Bachmann, and A. Burgisser (2012). “Insights into shallow magma storage and crystallization at Volcán Llaima (Andean Southern Volcanic Zone, Chile)”. *Journal of Volcanology and Geothermal Research* 211–212, pages 76–91. DOI: [10.1016/j.jvolgeores.2011.09.010](https://doi.org/10.1016/j.jvolgeores.2011.09.010).
- Buckland, H. M., K. V. Cashman, S. L. Engwell, and A. C. Rust (2020). “Sources of uncertainty in the Mazama isopachs and the implications for interpreting distal tephra deposits from large magnitude eruptions”. *Bulletin of Volcanology* 82(3). DOI: [10.1007/s00445-020-1362-1](https://doi.org/10.1007/s00445-020-1362-1).
- Buckland, H. M., L. G. Mastin, S. L. Engwell, and K. V. Cashman (2022). “Modelling the transport and deposition of ash following a magnitude 7 eruption: the distal Mazama tephra”. *Bulletin of Volcanology* 84(9). DOI: [10.1007/s00445-022-01593-1](https://doi.org/10.1007/s00445-022-01593-1).
- Buckland, H. M., J. Saxby, M. Roche, P. Meredith, A. C. Rust, K. V. Cashman, and S. L. Engwell (2021). “Measuring the size of non-spherical particles and the implications for grain size analysis in volcanology”. *Journal of Volcanology and Geothermal Research* 415, page 107257. DOI: [10.1016/j.jvolgeores.2021.107257](https://doi.org/10.1016/j.jvolgeores.2021.107257).
- Cashman, K. V. (1992). “Groundmass crystallization of Mount St. Helens dacite, 1980?1986: a tool for interpreting shallow magmatic processes”. *Contributions to Mineralogy and Petrology* 109(4), pages 431–449. DOI: [10.1007/bf00306547](https://doi.org/10.1007/bf00306547).
- (2020). “Crystal Size Distribution (CSD) Analysis of Volcanic Samples: Advances and Challenges”. *Frontiers in Earth Science* 8. DOI: [10.3389/feart.2020.00291](https://doi.org/10.3389/feart.2020.00291).
- Cashman, K. V. and G. Giordano (2014). “Calderas and magma reservoirs”. *Journal of Volcanology and Geothermal Research* 288, pages 28–45. DOI: [10.1016/j.jvolgeores.2014.09.007](https://doi.org/10.1016/j.jvolgeores.2014.09.007).
- Cashman, K. V. and R. P. Hoblitt (2004). “Magmatic precursors to the 18 May 1980 eruption of Mount St. Helens, USA”. *Geology* 32(2), page 141. DOI: [10.1130/g20078.1](https://doi.org/10.1130/g20078.1).
- Cashman, K. V. and S. M. McConnell (2005). “Multiple levels of magma storage during the 1980 summer eruptions of Mount St. Helens, WA”. *Bulletin of Volcanology* 68(1), pages 57–75. DOI: [10.1007/s00445-005-0422-x](https://doi.org/10.1007/s00445-005-0422-x).
- Cassidy, M. and L. Mani (2022). “Huge volcanic eruptions: time to prepare”. *Nature* 608(7923), pages 469–471. DOI: [10.1038/d41586-022-02177-x](https://doi.org/10.1038/d41586-022-02177-x).
- Cassidy, M., J. M. Castro, C. Helo, V. R. Troll, F. M. Deegan, D. Muir, D. A. Neave, and S. P. Mueller (2016). “Volatile dilution during magma injections and implications for volcano explosivity”. *Geology* 44(12), pages 1027–1030. DOI: [10.1130/g38411.1](https://doi.org/10.1130/g38411.1).
- Cassidy, M., P. Cole, K. E. Hicks, N. R. Varley, N. Peters, and A. H. Lerner (2015). “Rapid and slow: Varying magma ascent rates as a mechanism for Vulcanian explosions”. *Earth and Planetary Science Letters* 420, pages 73–84. DOI: [10.1016/j.epsl.2015.03.025](https://doi.org/10.1016/j.epsl.2015.03.025).
- Cioni, R., L. Gurioli, A. Sbrana, and G. Vougioukalakis (2000). “Precursory phenomena and destructive events related to the Late Bronze Age Minoan (Thera, Greece) and AD 79 (Vesuvius, Italy) Plinian eruptions; inferences from the

- stratigraphy in the archaeological areas". *Geological Society, London, Special Publications* 171(1), pages 123–141. DOI: [10.1144/gsl.sp.2000.171.01.11](https://doi.org/10.1144/gsl.sp.2000.171.01.11).
- Cioni, R., M. Pistolesi, A. Bertagnini, C. Bonadonna, A. Hoskuldsson, and B. Scateni (2014). "Insights into the dynamics and evolution of the 2010 Eyjafjallajökull summit eruption (Iceland) provided by volcanic ash textures". *Earth and Planetary Science Letters* 394, pages 111–123. DOI: [10.1016/j.epsl.2014.02.051](https://doi.org/10.1016/j.epsl.2014.02.051).
- Clarke, A., S. Stephens, R. Teasdale, R. Sparks, and K. Diller (2007). "Petrologic constraints on the decompression history of magma prior to Vulcanian explosions at the Soufrière Hills volcano, Montserrat". *Journal of Volcanology and Geothermal Research* 161(4), pages 261–274. DOI: [10.1016/j.jvolgeores.2006.11.007](https://doi.org/10.1016/j.jvolgeores.2006.11.007).
- Cooper, K. M. and A. J. R. Kent (2014). "Rapid remobilization of magmatic crystals kept in cold storage". *Nature* 506(7489), pages 480–483. DOI: [10.1038/nature12991](https://doi.org/10.1038/nature12991).
- Coote, A. C. and P. Shane (2016). "Crystal origins and magmatic system beneath Ngauruhoe volcano (New Zealand) revealed by plagioclase textures and compositions". *Lithos* 260, pages 107–119. DOI: [10.1016/j.lithos.2016.05.017](https://doi.org/10.1016/j.lithos.2016.05.017).
- D'Arcy Wood, G. (2015). *Tambora: The Eruption That Changed the World*. Princeton University Press. ISBN: 9781400851409. DOI: [10.1515/9781400851409](https://doi.org/10.1515/9781400851409).
- Decker, R. W. (1986). "Forecasting Volcanic Eruptions". *Annual Review of Earth and Planetary Sciences* 14(1), pages 267–291. DOI: [10.1146/annurev.ea.14.050186.001411](https://doi.org/10.1146/annurev.ea.14.050186.001411).
- Druitt, T. H. (2014). "New insights into the initiation and venting of the Bronze-Age eruption of Santorini (Greece), from component analysis". *Bulletin of Volcanology* 76(2). DOI: [10.1007/s00445-014-0794-x](https://doi.org/10.1007/s00445-014-0794-x).
- Druitt, T. H. and C. R. Bacon (1986). "Lithic breccia and ignimbrite erupted during the collapse of Crater Lake Caldera, Oregon". *Journal of Volcanology and Geothermal Research* 29(1–4), pages 1–32. DOI: [10.1016/0377-0273\(86\)90038-7](https://doi.org/10.1016/0377-0273(86)90038-7).
- (1989). "Petrology of the zoned calcalkaline magma chamber of Mount Mazama, Crater Lake, Oregon". *Contributions to Mineralogy and Petrology* 101(2), pages 245–259. DOI: [10.1007/bf00375310](https://doi.org/10.1007/bf00375310).
- Dunbar, N. W., G. K. Jacobs, and M. T. Naney (1995). "Crystallization processes in an artificial magma: variations in crystal shape, growth rate and composition with melt cooling history". *Contributions to Mineralogy and Petrology* 120(3–4), pages 412–425. DOI: [10.1007/bf00306518](https://doi.org/10.1007/bf00306518).
- Edmonds, M. (2001). "A model for degassing at the Soufrière Hills Volcano, Montserrat, West Indies, based on geochemical data". *Earth and Planetary Science Letters* 186(2), pages 159–173. DOI: [10.1016/s0012-821x\(01\)00242-4](https://doi.org/10.1016/s0012-821x(01)00242-4).
- Egan, J., R. Staff, and J. Blackford (2015). "A high-precision age estimate of the Holocene Plinian eruption of Mount Mazama, Oregon, USA". *The Holocene* 25(7), pages 1054–1067. DOI: [10.1177/0959683615576230](https://doi.org/10.1177/0959683615576230).
- Eychenne, J., K. V. Cashman, A. Rust, and A. Durant (2015). "Impact of the lateral blast on the spatial pattern and grain size characteristics of the 18 May 1980 Mount St. Helens fall-out deposit". *Journal of Geophysical Research: Solid Earth* 120(9), pages 6018–6038. DOI: [10.1002/2015jb012116](https://doi.org/10.1002/2015jb012116).
- Flaherty, T., T. H. Druitt, L. Francalanci, P. Schiano, and O. Sigmarsson (2022). "Temporal variations in the diversity of primitive melts supplied to the Santorini silicic magmatic system and links to lithospheric stresses". *Contributions to Mineralogy and Petrology* 177(8). DOI: [10.1007/s00410-022-01941-6](https://doi.org/10.1007/s00410-022-01941-6).
- Flaherty, T., T. H. Druitt, H. Tuffen, M. D. Higgins, F. Costa, and A. Cadoux (2018). "Multiple timescale constraints for high-flux magma chamber assembly prior to the Late Bronze Age eruption of Santorini (Greece)". *Contributions to Mineralogy and Petrology* 173(9). DOI: [10.1007/s00410-018-1490-1](https://doi.org/10.1007/s00410-018-1490-1).
- Fontijn, K., H. Rawson, M. Van Daele, J. Moernaut, A. M. Abarzúa, K. Heirman, S. Bertrand, D. M. Pyle, T. A. Mather, M. De Batist, J.-A. Naranjo, and H. Moreno (2016). "Synchronisation of sedimentary records using tephra: A post-glacial tephrochronological model for the Chilean Lake District". *Quaternary Science Reviews* 137, pages 234–254. DOI: [10.1016/j.quascirev.2016.02.015](https://doi.org/10.1016/j.quascirev.2016.02.015).
- Gaunt, H. E., B. Bernard, S. Hidalgo, A. Proaño, H. Wright, P. Mothes, E. Criollo, and U. Kueppers (2016). "Juvenile magma recognition and eruptive dynamics inferred from the analysis of ash time series: The 2015 reawakening of Cotopaxi volcano". *Journal of Volcanology and Geothermal Research* 328, pages 134–146. DOI: [10.1016/j.jvolgeores.2016.10.013](https://doi.org/10.1016/j.jvolgeores.2016.10.013).
- Global Volcanism Program (2022). "Report on Hunga Tonga-Hunga Ha'apai (Tonga)". *Bulletin of the Global Volcanism Network* 47(2). Edited by A. E. Crafford and E. Venzke. DOI: [10.5479/si.gvp.bgvn202202-243040](https://doi.org/10.5479/si.gvp.bgvn202202-243040).
- Gualda, G. A. R., M. S. Ghiorso, R. V. Lemons, and T. L. Carley (2012). "Rhyolite-MELTS: a Modified Calibration of MELTS Optimized for Silica-rich, Fluid-bearing Magmatic Systems". *Journal of Petrology* 53(5), pages 875–890. DOI: [10.1093/petrology/egr080](https://doi.org/10.1093/petrology/egr080).
- Gupta, A. K., R. Bennartz, K. E. Fauria, and T. Mittal (2022). "Eruption chronology of the December 2021 to January 2022 Hunga Tonga-Hunga Ha'apai eruption sequence". *Communications Earth & Environment* 3(1). DOI: [10.1038/s43247-022-00606-3](https://doi.org/10.1038/s43247-022-00606-3).
- Hammer, J. E., K. V. Cashman, R. P. Hoblitt, and S. Newman (1999). "Degassing and microlite crystallization during pre-climactic events of the 1991 eruption of Mt. Pinatubo, Philippines". *Bulletin of Volcanology* 60(5), pages 355–380. DOI: [10.1007/s004450050238](https://doi.org/10.1007/s004450050238).
- Harris, A. J. L., L. Gurioli, E. E. Hughes, and S. Lagreulet (2012). "Impact of the Eyjafjallajökull ash cloud: A newspaper perspective". *Journal of Geophysical Research: Solid Earth* 117(B9). DOI: [10.1029/2011jb008735](https://doi.org/10.1029/2011jb008735).
- Hoblitt, R. P. (1996). "The preclimactic eruptions of Mount Pinatubo, June 1991". *Fire and Mud: eruptions and lahars of Mount Pinatubo, Philippines*. Edited by C. G. Newhall and A. S. Punongbayan. Philippine Institute of Volcanology, Seismology, Quezon City, and University of Washington Press, Seattle, pages 457–511.

- Humphreys, M. C., M. Edmonds, and M. S. Klöcking (2016). “The validity of plagioclase-melt geothermometry for degassing-driven magma crystallization”. *American Mineralogist* 101(4), pages 769–779. DOI: [10.2138/am-2016-5314](https://doi.org/10.2138/am-2016-5314).
- Jones, T. J., J. K. Russell, R. J. Brown, and L. Hollendonner (2022). “Melt stripping and agglutination of pyroclasts during the explosive eruption of low viscosity magmas”. *Nature Communications* 13(1). DOI: [10.1038/s41467-022-28633-w](https://doi.org/10.1038/s41467-022-28633-w).
- Kamata, H., K. Suzuki-Kamata, and C. R. Bacon (1993). “Deformation of the Wineglass Welded Tuff and the timing of caldera collapse at Crater Lake, Oregon”. *Journal of Volcanology and Geothermal Research* 56(3), pages 253–265. DOI: [10.1016/0377-0273\(93\)90019-n](https://doi.org/10.1016/0377-0273(93)90019-n).
- Karlstrom, L., M. L. Rudolph, and M. Manga (2012). “Caldera size modulated by the yield stress within a crystal-rich magma reservoir”. *Nature Geoscience* 5(6), pages 402–405. DOI: [10.1038/ngeo1453](https://doi.org/10.1038/ngeo1453).
- Karlstrom, L., H. M. Wright, and C. R. Bacon (2015). “The effect of pressurized magma chamber growth on melt migration and pre-caldera vent locations through time at Mount Mazama, Crater Lake, Oregon”. *Earth and Planetary Science Letters* 412, pages 209–219. DOI: [10.1016/j.epsl.2014.12.001](https://doi.org/10.1016/j.epsl.2014.12.001).
- Kelly, L. J., K. E. Fauria, M. Manga, S. J. Cronin, F. H. Latu'ila, J. Paredes-Mariño, T. Mittal, and R. Bennartz (2024). “Airfall volume of the 15 January 2022 eruption of Hunga volcano estimated from ocean color changes”. *Bulletin of Volcanology* 86(6). DOI: [10.1007/s00445-024-01744-6](https://doi.org/10.1007/s00445-024-01744-6).
- Kilgour, G., J. Blundy, K. V. Cashman, and H. M. Mader (2013). “Small volume andesite magmas and melt–mush interactions at Ruapehu, New Zealand: evidence from melt inclusions”. *Contributions to Mineralogy and Petrology* 166(2), pages 371–392. DOI: [10.1007/s00410-013-0880-7](https://doi.org/10.1007/s00410-013-0880-7).
- Kratzmann, D. J., S. N. Carey, J. Fero, R. A. Scasso, and J.-A. Naranjo (2010). “Simulations of tephra dispersal from the 1991 explosive eruptions of Hudson volcano, Chile”. *Journal of Volcanology and Geothermal Research* 190(3–4), pages 337–352. DOI: [10.1016/j.jvolgeores.2009.11.021](https://doi.org/10.1016/j.jvolgeores.2009.11.021).
- Liu, E. J., K. V. Cashman, E. Miller, H. Moore, M. Edmonds, B. E. Kunz, F. Jenner, and G. Chigna (2020). “Petrologic monitoring at Volcán de Fuego, Guatemala”. *Journal of Volcanology and Geothermal Research* 405, page 107044. DOI: [10.1016/j.jvolgeores.2020.107044](https://doi.org/10.1016/j.jvolgeores.2020.107044).
- Long, C. J., M. J. Power, T. A. Minckley, and A. L. Hass (2014). “The impact of Mt Mazama tephra deposition on forest vegetation in the Central Cascades, Oregon, USA”. *The Holocene* 24(4), pages 503–511. DOI: [10.1177/0959683613520258](https://doi.org/10.1177/0959683613520258).
- Madden-Nadeau, A., M. Cassidy, D. Pyle, T. Mather, S. Watt, S. Engwell, M. Abdurrachman, M. Nurshal, D. Tappin, and T. Ismail (2021). “The magmatic and eruptive evolution of the 1883 caldera-forming eruption of Krakatau: Integrating field- to crystal-scale observations”. *Journal of Volcanology and Geothermal Research* 411, page 107176. DOI: [10.1016/j.jvolgeores.2021.107176](https://doi.org/10.1016/j.jvolgeores.2021.107176).
- Mandeville, C. W., J. D. Webster, C. Tappen, B. E. Taylor, A. Timbal, A. Sasaki, E. Hauri, and C. R. Bacon (2009). “Stable isotope and petrologic evidence for open-system degassing during the climactic and pre-climactic eruptions of Mt. Mazama, Crater Lake, Oregon”. *Geochimica et Cosmochimica Acta* 73(10), pages 2978–3012. DOI: [10.1016/j.gca.2009.01.019](https://doi.org/10.1016/j.gca.2009.01.019).
- Martel, C. (2012). “Eruption Dynamics Inferred from Micro-lite Crystallization Experiments: Application to Plinian and Dome-forming Eruptions of Mt. Pelee (Martinique, Lesser Antilles)”. *Journal of Petrology* 53(4), pages 699–725. DOI: [10.1093/petrology/egr076](https://doi.org/10.1093/petrology/egr076).
- Matsumoto, K. and N. Geshi (2021). “Shallow crystallization of eruptive magma inferred from volcanic ash microtextures: a case study of the 2018 eruption of Shinmoedake volcano, Japan”. *Bulletin of Volcanology* 83(5). DOI: [10.1007/s00445-021-01451-6](https://doi.org/10.1007/s00445-021-01451-6).
- McNamara, K., K. V. Cashman, A. C. Rust, K. Fontijn, F. Chalié, E. L. Tomlinson, and G. Yirgu (2018). “Using Lake Sediment Cores to Improve Records of Volcanism at Aluto Volcano in the Main Ethiopian Rift”. *Geochemistry, Geophysics, Geosystems* 19(9), pages 3164–3188. DOI: [10.1029/2018gc007686](https://doi.org/10.1029/2018gc007686).
- Mehring, P. J., E. Blinman, and K. L. Petersen (1977). “Pollen Influx and Volcanic Ash: The pollen content of Mazama and Glacier Peak ashes reveals details of their depositional chronologies.” *Science* 198(4314), pages 257–261. DOI: [10.1126/science.198.4314.257](https://doi.org/10.1126/science.198.4314.257).
- Miwa, T., N. Geshi, and H. Shinohara (2013). “Temporal variation in volcanic ash texture during a vulcanian eruption at the Sakurajima volcano, Japan”. *Journal of Volcanology and Geothermal Research* 260, pages 80–89. DOI: [10.1016/j.jvolgeores.2013.05.010](https://doi.org/10.1016/j.jvolgeores.2013.05.010).
- Myers, M. L., D. J. Geist, M. C. Rowe, K. S. Harpp, P. J. Wallace, and J. Dufek (2014). “Replenishment of volatile-rich mafic magma into a degassed chamber drives mixing and eruption of Tungurahua volcano”. *Bulletin of Volcanology* 76(11). DOI: [10.1007/s00445-014-0872-0](https://doi.org/10.1007/s00445-014-0872-0).
- Myers, M. L., P. J. Wallace, C. J. Wilson, B. K. Morter, and E. J. Swallow (2016). “Prolonged ascent and episodic venting of discrete magma batches at the onset of the Huckleberry Ridge supereruption, Yellowstone”. *Earth and Planetary Science Letters* 451, pages 285–297. DOI: [10.1016/j.epsl.2016.07.023](https://doi.org/10.1016/j.epsl.2016.07.023).
- Newhall, C., S. Self, and A. Robock (2018). “Anticipating future Volcanic Explosivity Index (VEI) 7 eruptions and their chilling impacts”. *Geosphere* 14(2), pages 572–603. DOI: [10.1130/ges01513.1](https://doi.org/10.1130/ges01513.1).
- O'Connor, J. E., P. F. McDowell, P. Lind, C. G. Rasmussen, and M. K. Keith (2015). *Geomorphology and flood-plain vegetation of the Sprague and lower Sycan Rivers, Klamath Basin, Oregon*. DOI: [10.3133/sir20145223](https://doi.org/10.3133/sir20145223).
- O'Donnell, S. B. and J. E. Gardner (2022). “Microlite crystallization during eruptions at Mt. Mazama: implications for magma ascent”. *Contributions to Mineralogy and Petrology* 177(11). DOI: [10.1007/s00410-022-01971-0](https://doi.org/10.1007/s00410-022-01971-0).
- Oetelaar, G. A. and A. B. Beaudoin (2005). “Darkened Skies and Sparkling Grasses: The Potential Impact of the Mazama Ash

- Fall on the Northwestern Plains". *Plains Anthropologist* 50(195), pages 285–305. DOI: [10.1179/pan.2005.026](https://doi.org/10.1179/pan.2005.026).
- Oetelaar, G. A. and A. B. Beaudoin (2016). "Evidence of cultural responses to the impact of the Mazama ash fall from deeply stratified archaeological sites in southern Alberta, Canada". *Quaternary International* 394, pages 17–36. DOI: [10.1016/j.quaint.2014.08.015](https://doi.org/10.1016/j.quaint.2014.08.015).
- Pistolesi, M., R. Cioni, C. Bonadonna, M. Elisondo, V. Baumann, A. Bertagnini, L. Chiari, R. Gonzales, M. Rosi, and L. Francalanci (2015). "Complex dynamics of small-moderate volcanic events: the example of the 2011 rhyolitic Cordón Caulle eruption, Chile". *Bulletin of Volcanology* 77(1). DOI: [10.1007/s00445-014-0898-3](https://doi.org/10.1007/s00445-014-0898-3).
- Pistolesi, M., M. Rosi, R. Cioni, K. V. Cashman, A. Rossotti, and E. Aguilera (2011). "Physical volcanology of the post-twelfth-century activity at Cotopaxi volcano, Ecuador: Behavior of an andesitic central volcano". *Geological Society of America Bulletin* 123(5–6), pages 1193–1215. DOI: [10.1130/b30301.1](https://doi.org/10.1130/b30301.1).
- Preece, K., F. van der Zwan, J. Hammer, and R. Gertisser (2023). "A Textural Perspective on the Magmatic System and Eruptive Behaviour of Merapi Volcano". *Merapi Volcano*. Springer International Publishing, pages 265–289. ISBN: 9783031150401. DOI: [10.1007/978-3-031-15040-1\\_9](https://doi.org/10.1007/978-3-031-15040-1_9).
- Pyle, D. M. (1989). "The thickness, volume and grain size of tephra fall deposits". *Bulletin of Volcanology* 51(1), pages 1–15. DOI: [10.1007/bf01086757](https://doi.org/10.1007/bf01086757).
- (2000). "Sizes of Volcanic Eruptions". *The Encyclopedia of Volcanoes*. Edited by H. Sigurdsson and B. Houghton. First edition. Amsterdam: Academic Press, pages 257–264. ISBN: 9780126431407. DOI: [10.1016/b978-0-12-385938-9.00013-4](https://doi.org/10.1016/b978-0-12-385938-9.00013-4).
- Rosi, M., L. Vezzoli, A. Castelmennano, and G. Grieco (1999). "Plinian pumice fall deposit of the Campanian Ignimbrite eruption (Phlegraean Fields, Italy)". *Journal of Volcanology and Geothermal Research* 91(2–4), pages 179–198. DOI: [10.1016/s0377-0273\(99\)00035-9](https://doi.org/10.1016/s0377-0273(99)00035-9).
- Rougier, J., R. S. J. Sparks, K. V. Cashman, and S. K. Brown (2018). "The global magnitude–frequency relationship for large explosive volcanic eruptions". *Earth and Planetary Science Letters* 482, pages 621–629. DOI: [10.1016/j.epsl.2017.11.015](https://doi.org/10.1016/j.epsl.2017.11.015).
- Ruth, D. C. S., F. Costa, C. Bouvet de Maisonneuve, L. Franco, J. A. Cortés, and E. S. Calder (2018). "Crystal and melt inclusion timescales reveal the evolution of magma migration before eruption". *Nature Communications* 9(1). DOI: [10.1038/s41467-018-05086-8](https://doi.org/10.1038/s41467-018-05086-8).
- Saunders, K., J. Blundy, R. Dohmen, and K. V. Cashman (2012). "Linking Petrology and Seismology at an Active Volcano". *Science* 336(6084), pages 1023–1027. DOI: [10.1126/science.1220066](https://doi.org/10.1126/science.1220066).
- Shamloo, H. I. and C. B. Till (2019). "Decadal transition from quiescence to supereruption: petrologic investigation of the Lava Creek Tuff, Yellowstone Caldera, WY". *Contributions to Mineralogy and Petrology* 174(4). DOI: [10.1007/s00410-019-1570-x](https://doi.org/10.1007/s00410-019-1570-x).
- Simkin, T. and R. S. Fiske (1983). "Krakatau 1883". *Earthquake Information Bulletin (USGS)* 15(4), pages 128–133.
- Sparks, R. (2003). "Forecasting volcanic eruptions". *Earth and Planetary Science Letters* 210(1–2), pages 1–15. DOI: [10.1016/s0012-821x\(03\)00124-9](https://doi.org/10.1016/s0012-821x(03)00124-9).
- Stock, M. J., M. C. S. Humphreys, V. C. Smith, R. Isaia, and D. M. Pyle (2016). "Late-stage volatile saturation as a potential trigger for explosive volcanic eruptions". *Nature Geoscience* 9(3), pages 249–254. DOI: [10.1038/ngeo2639](https://doi.org/10.1038/ngeo2639).
- Stothers, R. B. (1984). "The Great Tambora Eruption in 1815 and Its Aftermath". *Science* 224(4654), pages 1191–1198. DOI: [10.1126/science.224.4654.1191](https://doi.org/10.1126/science.224.4654.1191).
- Suzuki, Y., M. Nagai, F. Maeno, A. Yasuda, N. Hokanishi, T. Shimano, M. Ichihara, T. Kaneko, and S. Nakada (2013). "Precursory activity and evolution of the 2011 eruption of Shinmoe-dake in Kirishima volcano—insights from ash samples". *Earth, Planets and Space* 65(6), pages 591–607. DOI: [10.5047/eps.2013.02.004](https://doi.org/10.5047/eps.2013.02.004).
- Swallow, E. J., C. J. N. Wilson, M. L. Myers, P. J. Wallace, K. S. Collins, and E. G. C. Smith (2018). "Evacuation of multiple magma bodies and the onset of caldera collapse in a supereruption, captured in glass and mineral compositions". *Contributions to Mineralogy and Petrology* 173(4). DOI: [10.1007/s00410-018-1459-0](https://doi.org/10.1007/s00410-018-1459-0).
- Symons, G. (1888). *Quarterly Journal of the Royal Meteorological Society* 14(68), pages 301–307. DOI: [10.1002/qj.4970146809](https://doi.org/10.1002/qj.4970146809).
- Taddeucci, J., M. Pompilio, and P. Scarlato (2004). "Conduit processes during the July–August 2001 explosive activity of Mt. Etna (Italy): inferences from glass chemistry and crystal size distribution of ash particles". *Journal of Volcanology and Geothermal Research* 137(1–3), pages 33–54. DOI: [10.1016/j.jvolgeores.2004.05.011](https://doi.org/10.1016/j.jvolgeores.2004.05.011).
- Vásconez Müller, A., K. V. Cashman, S. J. Mitchell, and F. J. Vasconez (2022). "The 2.6–2.3 ka explosive eruptive period of the Pululahua dome complex, Ecuador: insights from pyroclast analysis". *Bulletin of Volcanology* 84(8). DOI: [10.1007/s00445-022-01590-4](https://doi.org/10.1007/s00445-022-01590-4).
- Verbeek, R. D. M. (1885). *Krakatau*. Imprimerie de l'état, Batavia.
- Vinkler, A. P., K. V. Cashman, G. Giordano, and G. Groppelli (2012). "Evolution of the mafic Villa Senni caldera-forming eruption at Colli Albani volcano, Italy, indicated by textural analysis of juvenile fragments". *Journal of Volcanology and Geothermal Research* 235–236, pages 37–54. DOI: [10.1016/j.jvolgeores.2012.03.006](https://doi.org/10.1016/j.jvolgeores.2012.03.006).
- Waters, L. E., B. J. Andrews, and R. A. Lange (2015). "Rapid Crystallization of Plagioclase Phenocrysts in Silicic Melts during Fluid-saturated Ascent: Phase Equilibrium and Decompression Experiments". *Journal of Petrology* 56(5), pages 981–1006. DOI: [10.1093/petrology/egv025](https://doi.org/10.1093/petrology/egv025).
- Wiejaczka, J. and T. Giachetti (2022). "Using Eruption Source Parameters and High-Resolution Grain-Size Distributions of the 7.7 ka Cleetwood Eruption of Mount Mazama (Oregon, United States) to Reveal Primary and Secondary Eruptive Processes". *Frontiers in Earth Science* 10. DOI: [10.3389/feart.2022.853021](https://doi.org/10.3389/feart.2022.853021).



- Williams, H. (1942). *The Geology of Crater Lake National Park, Oregon: with a reconnaissance of the cascade range southward to Mount Shasta*. Carnegie Institution of Washington.
- Wright, H. M. N., C. R. Bacon, J. A. Vazquez, and T. W. Sisson (2012). “Sixty thousand years of magmatic volatile history before the caldera-forming eruption of Mount Mazama, Crater Lake, Oregon”. *Contributions to Mineralogy and Petrology* 164(6), pages 1027–1052. DOI: [10.1007/s00410-012-0787-8](https://doi.org/10.1007/s00410-012-0787-8).
- Wright, H. M. N., K. V. Cashman, M. Rosi, and R. Cioni (2007). “Breadcrust bombs as indicators of Vulcanian eruption dynamics at Guagua Pichincha volcano, Ecuador”. *Bulletin of Volcanology* 69(3), pages 281–300. DOI: [10.1007/s00445-006-0073-6](https://doi.org/10.1007/s00445-006-0073-6).
- Wright, H. M. N., R. Cioni, K. V. Cashman, P. Mothes, and M. Rosi (2023). “Decompression and degassing, repressurization, and regassing during cyclic eruptions at Guagua Pichincha volcano, Ecuador, 1999–2001”. *Bulletin of Volcanology* 85(2). DOI: [10.1007/s00445-023-01626-3](https://doi.org/10.1007/s00445-023-01626-3).
- Wright, H. M. N., J. S. Pallister, W. A. McCausland, J. P. Griswold, S. Andreastuti, A. Budianto, S. Primulyana, H. Gunawan, M. Battaglia, A. Diefenbach, J. Griswold, J. Ewert, P. Kelly, C. Kern, M. LaFevers, A. Lockhart, J. Marso, G. Mayberry, W. McCausland, J. Pallister, S. Schilling, R. Wessels, R. White, H. Wright, N. Aisyah, S. Andreastuti, A. Budianto, A. Heriwaseso, N. Kartadinata, Kristianto, S. Primulyana, R. Putra, U. B. Saing, A. Solihin, Y. Suparman, D. D. Syahbana, and H. Triastuty (2019). “Construction of probabilistic event trees for eruption forecasting at Sinabung volcano, Indonesia 2013–14”. *Journal of Volcanology and Geothermal Research* 382, pages 233–252. DOI: [10.1016/j.jvolgeores.2018.02.003](https://doi.org/10.1016/j.jvolgeores.2018.02.003).
- Young, S. R. (1990). “Physical volcanology of holocene airfall deposits from Mt Mazama, Crater Lake, Oregon.” PhD thesis. University of Lancaster.
- Zdanowicz, C. M., G. A. Zielinski, and M. S. Germani (1999). “Mount Mazama eruption: Calendrical age verified and atmospheric impact assessed”. *Geology* 27(7), page 621. DOI: [10.1130/0091-7613\(1999\)027<0621:mmecav>2.3.co;2](https://doi.org/10.1130/0091-7613(1999)027<0621:mmecav>2.3.co;2).